Osmotic Stress Activates Two Reactive Oxygen Species Pathways with Distinct Effects on Protein Nanodomains and Diffusion

Alexandre Martiniere, Jean Bernard Fiche, Marija Smokvarska, Stephane Mari, Carine Alcon, Xavier Dumont, Kian Hématy, Yvon Jaillais, Marcelo Nollmann, Christophe Maurel

Plant Physiology Preview. Published on February 4, 2019, as DOI:10.1104/pp.18.01065

Short title: ROS production effects protein nano-organisation

Osmotic stress activates two reactive oxygen species pathways with distinct effects on protein nanodomains and diffusion

Alexandre Martinière[a1]*, Jean Bernard Fiche[b]*, Marija Smokvarska[a], Stéphane Mari[a], Carine Alcon[a], Xavier Dumont[a], Kian Hematy[c], Yvon Jaillais[d], Marcelo Nollmann[b], Christophe Maurel[a]

[a] BPMP, CNRS, INRA, Montpellier SupAgro, Univ Montpellier, Montpellier, France

[b] Centre de Biochimie Structurale, CNRS UMR5048, INSERM U1054, Université de Montpellier, 29 rue de Navacelles, 34090 Montpellier, France

[c] Institut Jean-Pierre Bourgin, INRA, AgroParisTech, CNRS, Université Paris-Saclay, Versailles, France

[d] Laboratoire Reproduction et Développement des Plantes, Univ Lyon, ENS de Lyon, UCB Lyon 1, CNRS, INRA, F-69342 Lyon, France.

[1]Address correspondence to alexandre.martiniere@cnrs.fr

*contributed equally

One-sentence summary Hyperosmotic stress induces reorganization and increased diffusion of plasma membrane proteins by a specific ROS production pathway

AUTHOR CONTRIBUTIONS

AM, MS, CA, XD, KH and YJ preformed research; JBF and MN developed new analytic and computational tools; AM and SM design research; AM and CM wrote the paper.

ABSTRACT

Physiological acclimation of plants to an ever-changing environment is governed by complex combinatorial signaling networks that perceive and transduce various abiotic and biotic stimuli. Reactive oxygen species (ROS) serve as one of the second messengers in plant responses to hyperosmotic stress. The molecular bases of ROS production and the primary cellular processes that they target were investigated in the Arabidopsis (*Arabidopsis thaliana*) root. Combined pharmacological and genetic approaches showed that RESPIRATORY BURST OXIDASE HOMOLOG (RBOH) pathway and an additional pathway involving apoplastic ascorbate and iron can account for ROS production upon hyperosmotic stimulation. The two pathways determine synergistically the rate of membrane internalization, within minutes following activation. Live super-resolution microscopy revealed at single-molecule scale how ROS control specific diffusion and nano-organization of membrane cargo proteins. In particular, ROS generated by RBOHs initiated clustering of the PIP2;1 aquaporin and its removal from the plasma membrane. This process is contributed to by clathrin-mediated endocytosis, with a positive role of RBOH-dependent ROS, specifically under hyperosmotic stress.

INTRODUCTION

Terrestrial plants can experience dramatic changes in water availability when exposed to environmental challenges as diverse as drought, soil salinity, and fluctuations in air humidity or even temperature. To maintain their water status and acclimate to these environmental constraints, plants have evolved numerous physiological or developmental responses, including short-term regulation of stomatal aperture and tissue hydraulics and, on a longer term, alteration of root system architecture and leaf abscission. Despite their central role, the early cellular events that lead to these adaptive responses are largely unknown.

A few molecules and mechanisms that contribute, at least partially, to osmotic stress perception have emerged from recent studies. As first described in bacteria and now in plants, osmotic shocks result in mechanical stimuli that activate a group of nonselective mechanosensitive ion channels and help the cell to counteract excessive membrane tensions (Martinac et al., 1987; Hamilton et al., 2015b). In addition, the transmembrane histidine kinase ATHK1 was suggested to act as an osmosensor, similar to its yeast homolog (Urao et al., 1999). Finally, a direct genetic screen identified cations channels of the Reduced Hyperosmolality, Induced Ca2+ Increase 1/Calcium Permeable Stress-Gated Cation Channel 1 (OSCA/CSC1) gene family as mediating calcium influx during hyperosmotic stress (Hou et al., 2014; Yuan et al., 2014). Loss-of-function mutant plants showed a reduced stomata closure and altered root growth responses in stress conditions (Yuan et al., 2014).

Several types of second messengers are possibly involved, downstream of osmotic signal perception. For instance, a substantial apoplastic alkalization occurs concomitant to calcium influx in the first minutes following exposure of roots to salt (Choi et al., 2014; Guo et al., 2009; Gao et al., 2004; Stephan et al., 2016). Reactive oxygen species (ROS), which accumulate in the frame of tens of minutes following osmotic stress, also represent key second messengers during hyperosmotic signaling (Leshem et al., 2007). ROS signaling mediated by NADPH oxidases of the RESPIRATORY BURST OXIDASE HOMOLOG (RBOH) family are generally accepted as the dominant pathway in plants (Baxter et al., 2014; Mittler, 2017). By using the cytoplasmic pool of NADPH, these enzymes catalyze the production of apoplastic superoxide, which is further transformed into hydrogen peroxide by spontaneous dismutation or superoxide dismutase (SOD) activities (Figure 1A). Loss-of-function plants for *RBOHD* or *RBOHF* showed a reduced ROS accumulation in response to numerous environmental stimuli, including salt stress (Leshem et al., 2007). In addition,

rbohD or *rbohF* mutant plants displayed reduced proline accumulation in response to a long hyperosmotic treatment (Ben Rejeb et al., 2015). Thus, RBOHD or RBOHF represent good candidates for ROS production under osmotic stress

Osmotic stress exerts strong and rapid effects on cell membrane dynamics. Whereas membrane proteins should freely diffuse in the plane of the membrane due to thermal motion, a lot of plant plasma membrane (PM) proteins are essentially immobile (Martinière et al., 2012). This suggests an anchoring of these proteins to fix them in place. Within minutes following an osmotic or salt treatment, PLASMA MEMBRANE INTRINSIC PROTEIN 2;1 (PIP2;1) was found to start diffusing within the PM (Li et al., 2011; Hosy et al., 2015). High salt and sorbitol concentrations also enhance exchanges between the PM and endosomes within the same time frame. In particular, a strong bulk membrane internalization was revealed by FM4-64 uptake (Leshem et al., 2007; Zwiewka et al., 2015). In addition, all cargo proteins tested so far, among which the PIP2;1 aquaporin, PIN-FORMED 2 (PIN2) auxin transporter, and BRASSINOSTEROID INSENSITIVE 1 (BRI1) brassinosteroid receptor are depleted from the PM (Zwiewka et al., 2015; Li et al., 2011). Thus, osmotically induced bulk membrane internalization is thought to drive the removal of cargo proteins from the PM. Wudick et al. (2015) recently demonstrated that external application of hydrogen peroxide on root cells enhances PIP2;1 lateral diffusion and endocytosis, thereby mimicking the effects of a salt or hyperosmotic treatment (Wudick et al., 2015). A link between membrane dynamics and ROS signaling has also been demonstrated upon cryptogenin elicitation of tobacco (*Nicotiana tabacum*) BY2 cells. Cryptogenin induced clathrin-dependent endocytosis, and cells silenced for *NtRboh* had less clathrin foci at the PM than control ones (Leborgne-Castel et al., 2008). The exact mechanisms by which ROS act on membrane and cargo protein dynamics are not yet known.

In this work, we used Arabidopsis (*Arabidopsis thaliana*) roots to investigate early cell responses to osmotic stress. We focused on the molecular mechanisms of stress-induced production of ROS and their subsequent impact on PM dynamics. We identified, besides RBOH family members, another source of ROS involving ascorbate and iron (Fe). Whereas ROS play a general role in bulk endocytosis, we report on the behavior of individual membrane protein molecules and show that PIP2;1 nanodomain organization and endocytosis are strictly under the control of RBOH-dependent ROS. Super-resolution microscopy was used to further investigate the role of the clathrin machinery in these specific membrane dynamic responses.

109

110

111

RESULTS

RBOHs contribute only partially to osmotically induced ROS production.

Production in plant tissues of ROS, and superoxide (O_2^-) in particular, can be monitored through oxidation and enhanced fluorescence of dehydroethidum (DHE) dye (Figure 1B) (Tsukagoshi et al., 2010; Chen et al., 2013). A steady increase in fluorescence for up to 120 min was observed in 5-day-old plantlets incubated in the presence of DHE (Supplemental Figure 1). When plantlets were concomitantly treated with 300 mM sorbitol, the rate of DHE fluorescence increase was enhanced 2-fold (Supplemental Figure 1), within all cell types (Figure 1B). Hydroxyphenyl fluorescein (HPF), another ROS-sensitive dye that is mostly reactive with hydroxyl radicals (Tsukagoshi et al., 2010), revealed an essentially similar osmotic-stress-induced staining pattern (Supplemental Figure 2A). These observations conform to the idea that osmotic stress rapidly (i.e. within minutes) induces an overaccumulation of ROS in Arabidopsis roots.

Because the role of RBOH proteins was never formally tested in the context of osmotic stress, we used single (*rbohD* and *rbohF*) and double (*rbohD/F*) loss-of-function mutants. With respect to Col-0 plants, ROS accumulation in these genotypes was not altered in resting conditions. In contrast, the ROS response to sorbitol was partially reduced in each of the single mutants, with no further decrease in the *rbohD/F* double mutant (Figure 1C). The residual response of the latter plants suggested that other RBOH isoforms may be involved. Therefore, we used diphenylene iodonium (DPI), which inhibits all RBOHs by interacting with their flavin adenine dinucleotide (FAD) binding domain. In these experiments, plants were pretreated for 30 min with the inhibitor prior to staining with DHE for 15 min (Supplemental Figure 3). DPI slightly reduced ROS accumulation in Col-0 roots under resting conditions and partially inhibited the sorbitol-induced ROS response (compare Figure 1C and 1D). In contrast, the ROS response to sorbitol was fully insensitive to DPI in the *rbohF/D* double mutant (Figure 1F). These results show that RBOHD and F both contribute to osmotically induced ROS accumulation, though in a nonadditive manner. The data also show that an additional pathway, independent of RBOH, contributes to the osmotic-stress-induced ROS response.

Osmotically induced ROS production also involves reduced transition metals

O_2^- can also be produced, independently of NADPH oxidases, by a Haber-Weiss reaction whereby reduced transition metals transfer one electron to dioxygen (Figure 1E). To

investigate the contribution of this mechanism to ROS accumulation under osmotic stress, we treated plants with bathophenanthrolinedisulfonic acid (BPDS), a membrane-impermeant Fe^{2+} chelator that depletes free Fe^{2+} in the cell apoplasm. Whereas BPDS had no effect on DHE fluorescence in control conditions, it induced a significant reduction of ROS accumulation upon sorbitol treatment (Figure 1G).

Concomitant treatment of plants with DPI and BPDS resulted in a slight decrease in ROS accumulation in resting conditions and totally abolished the sorbitol effects (Figure 1G). When treated with BPDS, the *rbohD/F* double mutant also lost its sorbitol-induced ROS accumulation (Figure 1H). When HPF staining was used, a single pretreatment with DPI or BPDS totally inhibited the sorbitol-induced ROS response (Supplemental Figure 2B). These slight differences in response between DHE and HPF staining are likely due to their distinct sensitivity to the various ROS species (Tsukagoshi et al., 2010). Nevertheless, the overall data indicate that two ROS production pathways, mediated by RBOH and reduced iron, respectively, contribute to most of, if not all, the overaccumulation of ROS in Arabidopsis roots under osmotic stress.

A role of apoplastic ascorbate in ROS accumulation

Since reduced iron is considered to be almost absent in cells due to its very high toxicity, an iron reduction mechanism must be active during osmotic stress. We hypothesized that ascorbate could represent an alternative reducing agent (Grillet et al., 2014). Treatment of roots with purified ascorbate oxidase (AOX) did not alter DHE staining in resting conditions, whereas it reduced the sorbitol-induced response by around 20% (Figure 1G). When AOX was coincubated with DPI, the residual sorbitol-induced ROS accumulation was totally abolished (Figure 1G). These results suggest that, complementary to RBOHs, ascorbate is necessary to trigger ROS accumulation, probably in association with iron. To investigate this point further, we used a *vtc2.4* mutant that, with respect to Col-0, shows a reduction in ascorbate accumulation by two-thirds, without any major growth defect in standard condition (Grillet et al., 2014). Compared to Col-0, *vtc2.4* accumulated less ROS after osmotic stimulation; this response did not occur when plants were cotreated with DPI (Figure 1I). To confirm the limiting role of ascorbate in ROS accumulation, we applied 100 µM ascorbate onto roots and found a significant increase of ROS accumulation after 15 min (Figure 1J).

The results presented above were obtained after treatment with 300 mM sorbitol, which induces cell incipient plasmolysis (Supplemental Figure 4A). Under milder stress conditions

(100 mM sorbitol), cells experience a reduction in turgor with no major change in volume (Supplemental Figure 4A). Yet, this sorbitol treatment induced a ROS accumulation, of lower amplitude than with 300 mM, but with an essentially similar pharmacological inhibition profile. In particular, cotreatments with DPI and BPDS or DPI and AOX fully inhibited the osmotic response (Supplemental Figure 4B). These results indicate that the RBOH and iron/ascorbate pathways can be activated under a wide range of mild to pronounced osmotic stresses.

Due to their plasma membrane localization, RBOHD and F are expected to produce superoxide in the apoplasm. In addition, exogenously supplied AOX, which is marginally permeable to cell membranes, inhibited ROS accumulation (Figure 1G). Thus, the pool of ascorbate that contributes to osmotically induced ROS accumulation also seems to be localized in the apoplasm. To assess ROS accumulation in this compartment, we investigated DHE staining with confocal microscopy. In control conditions, oxidized DHE was localized in small dotted structures (Supplemental Figure 5, arrowheads) and in the nucleus (star). When cells were incubated with 300 mM sorbitol for 15 min, some staining was observed in the apoplasm (Supplemental Figure 5, arrows). These observations suggest that at least a part of the ROS accumulation triggered by osmotic stress takes place in this compartment.

The RBOH and iron/ascorbate pathways both contribute to activation of membrane internalization, but with distinct impacts on cargo proteins

Plant cells react to osmotic stress by modifying the rate of endocytosis. To investigate this process, we cotreated plants with the lipophilic fluorescent endocytic tracer FM4-64 and the fungal toxin Brefeldin A (BFA) and quantified the number of FM4-64-labeled BFA bodies per cell (Geldner et al., 2003). As expected, an increase in FM4-64 labeling of intracellular structures was observed in osmotically challenged plants (Figures 2A and 2B). In Col-0 plants treated with DPI or *rbohD/F* plants, intracellular labeling responses similar to those of Col-0 were observed under both control and sorbitol treatment conditions (Figures 2B and 2C). By comparison, Col-0 plants treated with BPDS showed a small decrease in osmotically induced FM4-64 labeling (Figure 2B). Moreover, a full inhibition of this response was observed when a BPDS treatment was coupled to pharmacological (Figures 2A and 2B) or genetic (Figure 2C) ablation of RBOH, using DPI or a *rbohD/F* genotype, respectively. Cell viability was checked after the experiment with fluorescein diacetate (FDA), with no visible effect of the inhibitors (Widholm, 1972) (Supplemental Figure 6). When the FM4-64 endocytotic index

from our whole set of measurements (Figure 2B and C) was plotted against corresponding DHE signals, a significant correlation was found (R^2=0.71) (Figure 2D). These results support the idea that ROS activate endocytosis (Leshem et al., 2007; Wudick et al., 2015). More specifically, they indicate that ROS, produced by both the RBOH and the ascorbate/Fe pathways, quantitatively contribute to the enhancement of cell endocytosis under osmotic stress.

While FM4-64 labeling reports on bulk membrane lipid internalization, we wondered whether cargo proteins follow the same route. We first investigated the P-type H^+-ATPase, PLASMA MEMBRANE PROTON ATPASE 2 (AHA2), as one of most abundant PM proteins (Gaxiola et al., 2007). For this, we used plants expressing a pro35S:GFP-AHA2 construct and counted the average number of GFP-labeled BFA compartments per cell as a proxy of AHA2 internalization. Surprisingly, this number was not enhanced but rather slightly decreased by a sorbitol treatment (Figures 2E and 2F). In agreement with previous observations in plants treated with salt or hydrogen peroxide (Li et al., 2011; Luu et al., 2012), root cells expressing a proPIP2;1:PIP2;1-GFP construct showed a higher number of GFP-labeled BFA bodies after a sorbitol treatment (Figures 2G and 2H). It was previously demonstrated that this is due to a higher endocytosis rate (Zwiewka et al., 2015). Interestingly, a DPI treatment fully suppressed the effect of osmotic stress on BFA body formation, while BPDS had no effects (Figure 2H). Thus, osmotic stress results in the selective endocytosis of certain cargos, which, in the case of PIP2;1, is fully dependent on RBOH-induced ROS accumulation.

Lateral diffusion of PIP2;1 and AHA2 is enhanced by osmotic stress but negatively controlled by ROS

Major changes in the mobility and distribution of PM proteins are thought to underlie their endocytosis. For instance, a hyperosmotic treatment can induce a substantial increase in PIP2;1 diffusion (Li et al., 2011; Hosy et al., 2015). Here, we wondered whether this process is under the control of ROS signaling, as suggested by previous experiments using hydrogen peroxide treatments (Wudick et al., 2015). A super-resolution microscopy approach called single-particle-tracking photoactivated localization microscopy (sptPALM) was used to visualize individual PIP2;1-mEOS molecules under total internal reflection fluorescence (TIRF) illumination in living cells (Hosy et al., 2015). In brief, the localization and displacement of several thousands of single molecules were reconstructed and used to assess the protein instantaneous diffusion constant (D) with a spatial resolution of around 30 nm and

temporal resolution of 20 ms (Figure 3A). For each reconstructed track, the mean square displacement (MSD) was computed and instantaneous diffusion coefficient was estimated with the help of homemade analysis software. In agreement with previous observations (Hosy et al., 2015), the diffusion of PIP2;1-mEOS within the PM was increased 2-fold after sorbitol treatment ($logD_{ctrl}$=-2.9, $logD_{sorbitol}$=-2.6, Figures 3B and 3C). While DPI or BPDS had no individual effects on AtPIP2;1-mEOS diffusion, both in the absence or presence of sorbitol, the combination of the two inhibitors markedly enhanced this parameter, specifically after a sorbitol treatment (Figure 3C). The overall results (Figure 2H and Figure 3C) suggest an opposite ROS dependency of PIP2;1 diffusion and endocytosis. At variance with PIP2;1 internalization, its diffusion under osmotic stress was negatively regulated by both the RBOHs and iron/ascorbate pathways

We used a similar sptPALM approach with transgenic lines expressing proUBQ10:mEOS2-AHA2 or proUBQ10:LTI6b-mEOS constructs to monitor diffusion within the PM of AHA2 and LOW TEMPERATURE INDUCED PROTEIN 6B (LTI6b), two proteins that are typically immobile or highly mobile, respectively (Figure 3 and Supplemental Figure 7). No change in diffusion of the already fast-diffusing LTI6b-mEOS molecules was observed after a sorbitol treatment (Supplemental Figure 7A and 7B). In contrast, diffusion of mEOS-AHA2, similar to that of PIP2;1-mEOS, was enhanced in these conditions (Figures 3D and 3E). Diffusion of mEOS-AHA2 was further enhanced by DPI and BPDS treatments, indicating that ROS accumulation generated by RBOHs or by the iron/ascorbate dependent pathway is acting as a negative regulator of mEOS2-AHA2 diffusion in sorbitol-treated plants (Figure 3F). Overall, the data show that increased diffusion of cargo proteins can be clearly dissociated from their endocytic behavior, questioning their causal relation.

PIP2;1, but not AHA2, shows enhanced RBOH-dependent clustering in response to osmotic stress.

Super-resolution imaging revealed that, in control conditions, PIP2;1-mEOS displayed a heterogeneous and sparse localization at the PM (Figure 4A). To test if this spatial organization corresponds to a random distribution or not, movies with a comparable density (3.20 tracks/µm²) were generated by simulation (Supplemental Figure 8A). The presence of clusters was assessed by calculating the local density of each track using a Vonoroi tessellation and comparing it to the one obtained in cells expressing PIP2;1-mEOS (Levet et al., 2015) (Supplemental Figures 8B and 8C). Whereas randomly generated data yielded a

narrow repartition of local densities peaking at 3.5 tracks/µm², PIP2;1-mEOS local density distribution was broader (Supplemental Figures 8B and 8C), reflecting the coexistence of sparse to very dense clusters (from 0.3 to 100 tracks/µm²). After a sorbitol treatment, PIP2;1-mEOS showed a shift towards higher local densities (Figure 4B and Supplemental Figure 8B), which was even appreciable from the super-resolution intensity images (Figure 4A). These results show that PIP2;1-mEOS molecules have a higher local density in response to a hyperosmotic treatment, but a similar number of PIP2;1-mEOS tracks per cell (Supplemental Figure 8A). To investigate how this phenomenon relates to other aspects of PIP2;1 dynamics (*e.g.* endocytosis and diffusion), we tested its dependency on ROS. Although the basal level of PIP2;1-mEOS clustering was sensitive to DPI, this inhibitor, but not BPDS, was able to prevent the enhancement of PIP2;1-mEOS local density by a hyperosmotic treatment (Figure 4C). When expressed in a *rbohD* background, which has a similarly impaired ROS production compared to *rbohF* or *rbohD/F* (Figure 1C), the pPIP:PIP2;1-mEOS construct yielded a reduced particle clustering and, most importantly, had become insensitive to osmotic treatment (Figure 4D). This inhibition profile matches the one obtained for PIP2;1 endocytosis (Figure 2H) and strongly suggests a causal chain linking, during osmotic stress, RBOH-dependent ROS accumulation, clustering of PIP2;1, and its eventual endocytosis.

mEOS2-AHA2 was also organized in small particle clusters, sparsely distributed in the PM (Figure 4E). Vonoroi tessellation indicated this clustering to be similar to the one obtained with pPIP:PIP2;1-mEOS-expressing plants (Figure 4F and Supplemental Figure 8B and 8C). In contrast, the local density of mEOS2-AHA2 was insensitive to a sorbitol treatment (Figures 4E and 4F). LTI6b-mEOS-expressing lines showed a higher local density of fluorescent particles that, however, were also insensitive to a sorbitol treatment (Supplemental Figure 7C). The data indicate that some cargo proteins, such as PIP2;1, at variance with others (AHA2 and LTI6b), are clustered in the PM and endocytosed upon a hyperosmotic treatment.

RbohD controls CLC2 diffusion in response to osmotic treatment

Previous reports indicate that part of PIP2;1 constitutive cycling occurs through clathrin-mediated endocytosis (CME) (Li et al., 2011; Luu et al., 2012; Ueda et al., 2016; Dhonukshe et al., 2007). For instance, PIP2;1-GFP showed a partial colocalization at the PM with CLATHRIN LIGHT CHAIN2 (CLC2) fused to mCherry (Li et al., 2011). Here, we expressed a pro35S:PIP2;1-GFP construct in proITAM>UAS-HUB1 plants (Dhonukshe et al., 2007). In the presence of tamoxifen, this line overaccumulates HUB1, a dominant-negative mutant form

of CLATHRIN HEAVY CHAIN1 (CHC1), thereby compromising clathrin coat assembly. BFA bodies labeled by GFP-PIP2;1 were rarely observed in tamoxifen-treated plants, whether they were treated or not by sorbitol (Figure 5A). Thus, PIP2;1-GFP is internalized mostly through CME, in both control and osmotic stress conditions. To estimate how a hyperosmotic treatment acts on CME, we generated Col-0 plants expressing proUBQ10:CLC2-mEOS used here as a core marker of the CME machinery (Konopka et al., 2008). Super-resolution imaging revealed that CLC2-mEOS was organized in clusters at the PM (Figure 5B) and that its local density was insensitive to a sorbitol treatment (Figure 5C). We also investigated the diffusion of individual CLC2-mEOS particles at the PM and its dependency on a sorbitol treatment. Tracks generated from sptPALM movies revealed two populations of CLC2 particles, with a low (~0.001 µm²/sec) and high (~0.1 µm²/sec) mean diffusion constant, respectively (Figure 5D). The repartition between these so-called mobile and immobile fractions was not altered after a sorbitol treatment (Figures 5E and 5G). In *rbohD* plants, however, a significant decrease of the CLC2-mEOS mobile fraction was induced by a hyperosmotic treatment (Figures 5F and 5G). These results suggest that CLC2-mEOS molecular dynamics are enhanced by RBOHD, specifically under osmotic stress. These effects may support the specific endocytosis of some PM-localized proteins, such as PIP2;1.

DISCUSSION

Upon perception of an osmotic imbalance, plant cells generate multiple secondary messengers, such as H^+, Ca^{2+}, and ROS, which in turn trigger a cascade of cell responses leading to physiological acclimation (Feng et al., 2016). In this work, we focused on ROS signaling, deciphered the molecular bases of their generation, and described their role in membrane dynamics and protein sorting at high resolution.

Two ROS-producing pathways contribute to ROS accumulation during osmotic signaling

RBOH proteins have emerged as central players of ROS signaling in plants. Here, we used pharmacological (DPI) and genetic tools (*rbohD* and *rbohF* mutants) to show their activation in the few minutes following hyperosmotic stimulation (Figure 6). We further show that RBOHD and RBOHF individually contribute to ROS accumulation, but in a nonadditive manner. These findings support previous work on the role of ROS and RBOH in long-term accumulation of proline in Arabidopsis roots under hyperosmotic stress (Ben Rejeb et al., 2015). More surprising was the finding that osmotically induced ROS accumulation is only partially dependent of the presence of functional RBOHs (Figures 1C and 1D), indicating the contribution of an additional mechanism for ROS production.

In these respects, our work points to a significant, but counterintuitive, role of ascorbate. As a reducing agent, ascorbate should primarily diminish ROS accumulation. This is typically the case when ascorbate fuels cytoplasmic peroxidases, like ASCORBATE PEROXIDASE 1 (APX1) (Davletova et al., 2005; Koussevitzky et al., 2008). Here, we found ascorbate to positively regulate ROS accumulation. Exogenous application of ascorbate on roots almost doubled the DHE signal; conversely, its genetic or pharmacological depletion decreased the fluorescent signal (Figures 1F-I). Since in the latter approach most of the exogenously supplied ascorbate oxidase (AOX) likely remains confined to the cell apoplasm, we propose that ascorbate mainly acts in this compartment during the hyperosmotic response. The finding that specific chelation of metals with BPDS reduced the DHE signal indicates that ascorbate would reduce transition metals, such as iron. The newly formed ferric iron would in turn promote the formation of superoxide from dioxygen through a Haber-Weiss reaction (Figure 1E). However, how can significant ascorbate levels be maintained in the cell apoplasm to sustain ROS production during osmotic treatment? An ascorbate efflux system at the cell PM, as was previously described in the context of iron nutrition in seeds (Grillet et al., 2014),

represents one possibility (Figure 6). Alternatively, cytoplasmic reducing power may be transferred through the cell membrane, by cytochrome proteins for instance, to regenerate the apoplastic dehydroascorbate (DHA) pool (Figure 6). Finally, an osmotically induced efflux of DHA can also be hypothesized (Figure 6). Interestingly, the balance between ascorbate and DHA in the apoplast has to be tightly controlled since misregulation of apoplastic ascorbate oxidases in tobacco plants altered hormonal and plant pathogen responses (Pignocchi et al., 2006). In line with this work, we also note that a polyamine oxidase was recently shown to act in a feedforward loop with RBOH proteins to regulate ROS production in stomata (Gémes et al., 2016). Thus, multiple ROS enzymes or generating mechanisms seem to work in concert during plant stress signaling. Whether these mechanisms are functionally redundant or convey some kind of response specificity remains largely unknown. This question was addressed here by analyzing membrane dynamics and protein sorting in root cells under hyperosmotic stress.

The two ROS-producing pathways contribute in synergy to lipid membrane internalization

Within seconds or tens of seconds, hyperosmotic conditions induce a loss of cell water and consequently a decrease in turgor. This results in instantaneous changes in cell shape, as well as PM tensions and invaginations (Oparka, 1994). Membrane cycling between the cell surface and intracellular compartments is simultaneously enhanced (Leshem et al., 2007; Luu et al., 2012; Zwiewka et al., 2015). Consistent with this model, we observed that an enhanced internalization of FM4-64 occurs in osmotically challenged root cells. We further demonstrated that lipid membrane internalization was correlated to superoxide accumulation (Figure 2) and that both inhibition of RBOH activities and iron chelation were necessary for total suppression of this process (Figures 2 B-C and Figure 6). While the data identify the two major sources of ROS involved in membrane reshaping, the mode of action of ROS on lipid membrane dynamics remains an intriguing question. ROS exert direct effects on phospholipid structure through peroxidation and can induce lipid-lipid cross-linking. These chemical effects could translate into changes in membrane biophysical properties, such as viscosity or curvature, and act on membrane internalization (Eichenberger et al., 1982; Bruch and Thayer, 1983). In addition, it cannot be excluded that ROS accumulation triggers formation of ordered microdomains at the PM to promote endocytosis, as was described in cells exposed to pathogen elicitors (Sandor et al., 2016).

Osmotically induced PIP2;1 endocytosis specifically controlled by ROS produced by RBOHs

While lipid membranes are largely internalized in response to a hyperosmotic challenge, we wondered whether protein cargoes would show the same movements. This seems to be case for the PIP2;1 aquaporin, which is internalized in response to a salt stress (Li et al., 2011; Luu et al., 2012), and showed here a similar response to a sorbitol hyperosmotic challenge. By contrast, endocytosis of the AHA2 H^+-ATPase was insensitive to the same treatment. Since AHA2 cycling is, along with AHA1, responsible for the maintenance of a proton gradient across the cell PM (Haruta and Sussman, 2012; Haruta et al., 2018), we speculate that this function has to be critically maintained for energizing turgor regulation under hyperosmotic conditions. Also unknown is the mechanism that allows selection of specific cargos for either internalization or retention.

Nevertheless, the most intriguing observation remained that, although RBOH and the ascorbate/iron pathway generate the same end product (superoxide), PIP2;1 internalization is selectively dependent on the former pathway (Figure 2H, Figure 4 C-D and Figure 6). Since ROS show short life spans (ms to sec for superoxide), limiting their diffusion to a restricted area, we propose that RBOHs create a ROS microenvironment in their vicinity, thereby acting on a specific protein subpopulation. Thus, the ROS-producing machinery rather than the produced species (superoxide) itself can determine signal specificity.

A recent study showed that in the Arabidopsis hypocotyl, RBOHD is depleted from the PM and degraded at 30 min after a 100 mM NaCl treatment (Hao et al., 2014). Since this response seems to be triggered by activation of RBOHD itself, a similar PM depletion might happen during osmotic stress. In addition, AtPIP2;1, which acts as a facilitator of hydrogen peroxide diffusion trough the PM (Rodrigues et al., 2017), could undergo co-endocytosis with RBOHD. This putative complex between aquaporins and NADPH oxidases might participate in regulation of cytoplasmic ROS.

Linking protein diffusion, clustering, and cycling

Previous studies, including ours, have investigated lateral protein diffusion at the PM, with the implicit idea that this phenomenon supports subsequent endocytosis (Wudick et al., 2015). Using a sptPALM approach, we investigated protein clustering as an additional prerequisite

for cellular endocytosis and tried to relate these different parameters with an unprecedented time and space resolution.

Most intrinsic PM proteins of plants, and PIPs especially, have a very low lateral diffusion (around 0.001 μm^2/sec). Yet, two recent reports have demonstrated that hyperosmotic and salt treatments can induce a substantial increase in PIP2;1 diffusion (Li et al., 2011; Hosy et al., 2015). In this work, we confirmed these results and extended them to AHA2, showing that, under a hyperosmotic treatment, both PIP2;1 and AHA2 shift to another organization through increased diffusion. In contrast, LTI6b diffusion and distribution were not modified in the same conditions. Thus, a hyperosmotic challenge can alter the lateral diffusion of some but not all PM proteins. Second, we found that neither RBOH nor the ascorbate/Fe ROS-generating system was required for cargo mobilization. In contrast, their inhibition enhanced protein diffusion under hyperosmotic conditions, showing that ROS rather act as negative regulators of their diffusion, maybe by lipid peroxidation (Figure 3).

This finding seems at variance with previous experiment showing that exposure of root cells to exogenous H_2O_2 enhanced PIP2;1 diffusion ((Wudick et al., 2015); our unpublished sptPALM data). Since production of apoplastic ROS is spatially regulated (see above) and involves complex interspecies conversion, we believe that these processes cannot be properly mimicked by treatment with exogenous H_2O_2. Overall, our comparative study of PIP2;1, AHA2, and LTI6b, together with ROS inhibition experiments, provides compelling evidence that an increase in protein diffusion is not linked to its subsequent endocytosis. More generally, protein diffusion may be corralled by PM /cell wall connections rather than being controlled by cellular ROS accumulation (Martiniere et al., 2011, Martiniere et al., 2013). These ideas led us to consider in closer detail protein clustering as another marker of protein behavior at the cell surface. The super-resolution microscopy approach indeed indicated that PIP2;1, AHA2, and LTI6b were not evenly distributed at the cell surface but were rather concentrated in small domains. After a hyperosmotic treatment, PIP2;1, but not AHA2 or LTI6b, showed higher clustering values, and this process was strictly RBOH dependent. These data perfectly match the endocytosis data, pointing to a causal link between higher clustering and enhanced endocytosis.

Our next question was about the mechanisms that drive PIP2;1 internalization, a process known to involve canonical clathrin-mediated endocytosis (CME) (Li et al., 2011). BFA experiments in plants expressing HUB1, a dominant-negative mutant form of CHC1,

confirmed this notion in the context of cell responses to hyperosmolarity (Figure 5A). Yet, inhibition of BFA compartment staining was only partial. Although we cannot exclude that conditional *HUB1* expression was not able to fully suppress CME, these partial effects may reflect, in agreement with previous work (Li et al., 2011; Wudick et al., 2015), an additional pathway for PIP2;1 internalization, independent of CME. Next, we investigated the effects of an osmotic stress on the molecular dynamics of CLC2, another major component of CME. CLC2-mEOS molecules showed two types of kinetic behavior, with either a high or a low diffusion. In animals, adaptor complex proteins (AP2) are known to bind to the PM by stochastic association with phosphatidylinositol two phosphates (PIP2), prior to clathrin-coated vesicle (CCV) initiation, growth, and maturation (Kadlecova et al., 2016). This binding induces an allosteric activation of the AP2 complex, thereby allowing interaction with clathrin triskelion (Jackson et al., 2010; Kelly et al., 2014). At this stage, cargo proteins can bind to AP2, and clathrin polymerization is primed. Alternatively, AP2/clathrin can dissociate from the PM. Due to its large size, the diffusion of CLC2-mEOS2 associated within CCV is supposed to be highly restricted. In contrast, when associated with PIP2/AP2/CLC complexes, CLC2-mEOS likely has a much higher diffusion coefficient. Thus, CLC2 diffusion can be used to reveal CCVs and the proportion of clathrin stochastic assemblies at the PM. In our experiments, the fraction of diffusible CLC2-mEOS was specifically reduced in *rbohD* under osmotic treatment, suggesting that clathrin stochastic assembly is perturbed in this context. Thus, the association between PIP2/AP2/CLC complexes and the PM might be supported by RBOHD-mediated ROS production, specifically in hyperosmotic conditions (Figure 6).

In conclusion, we have shown that PM dynamics are tightly controlled by cell signaling processes involving ROS, allowing the cell to respond to its osmotic environment. In our model, a hyperosmotic constraint activates RBOHs and a redox system coupling ascorbate and transition metals. The resulting ROS trigger overall cell membrane internalization. However, the nano-organization, lateral diffusion, and endocytosis of cargo proteins reveal highly specific behaviors and can be independently modulated depending on the cargo. While we demonstrate that an increase in protein lateral diffusion is not sufficient for triggering clustering and endocytosis, it will be interesting to see to what extent this upregulation remains necessary.

MATERIALS AND METHODS

Plant materials

The cDNAs of At4g30190 (*AHA2*) and At2g40060 (*CLC2*) were amplified by PCR and cloned into pENTR-D-TOPO (Invitrogen). The resulting constructs were used to generate N- or C-terminal fusions with mEOS, under the control of the *UBQ10* promoter (*ProUBQ10*), by cloning into pUBNEosFP and pUBCEosFP vectors, respectively (Grefen et al., 2010). The cDNA of At3g05890 (LTI6b-RCi2B) was cloned into pDONR207 by BP cloning. Multisite Gateway was then used to clone 2x35Sprom::LTI6b-mEos in pB7m34GW by LR recombination, using 2x35Sprom/pDONRP4RP1, LTI6bnoSTOP/pDONR207, and mEOS/pDONRP2RP3 as donor vectors (Karimi et al., 2007). mEOS/pDONRP2RP3 was obtained by amplifying mEOS and subsequent BP cloning into pDONRP2RP3 (Jaillais et al., 2011). Stable transformation of Arabidopsis (*Arabidopsis thaliana*) accession Col-0 was performed according to the floral dip method (Clough and Bent, 1998). proPIP2;1:PIP2;1-mEOS2 (Hosy et al., 2015) and proUBQ:CLC2-mEOS were also introduced into *rbohD* (Torres et al., 2002) by crossing. Arabidopsis plants expressing proPIP2;1:PIP2;1-GFP, proITAM>>HUB1, and mutants lines *RbohD*, *RbohF*, *RbohDxRbohF*, and *vtc2-4* were described elsewhere (Torres et al., 2002; Grillet et al., 2014; Wudick et al., 2015; Zwiewka et al., 2015).

Plant growth

Seeds were surface sterilized by agitation for 10 min in a solution containing 3.4 g/L BayroChlore and 0.02% Tween 20 detergent. Seeds were then rinsed 3 times with sterile water and sown on square plates containing half-strength Murashige and Skoog medium (MS/2) complemented with 2.5 mM 4-morpholineethanesulfonic acid (MES)-KOH, pH 6, and 1% sucrose. Plates were placed vertically in a growth chamber with 16 h light (200µmol m^{-2} s^{-1}) and 8 h dark cycles at 21°C and 70% of relative humidity for 5 days.

Osmotic and pharmacological treatments

Five-day-old Arabidopsis plantlets were bathed in a liquid MS/2 medium to allow recovery from transplanting. When indicated, 20 µM diphenyleneiodonium (DPI), 50 µM baptholphenanthrolinesulfonate (BPDS), 100 µM ascorbate, or 1.5 units/ml ascorbate oxidase (AOX) was included. After 30 min, plantlets were gently transferred for an additional 15 min

into a control MS/2 medium, in the absence or presence of 100 mM (mild osmotic stress) or 300 mM (severe osmotic stress) sorbitol, and with or without the corresponding inhibitors.

ROS measurements

The accumulation of O_2^- or hydroxyl radicals (·OH) was probed using 5 µM dihydroethidium (DHE) or 10 µM hydroxyphenyl fluorescein (HPF), respectively. The two dyes show increased fluorescence when oxidized. Observations were performed on the root elongation zone using a Zeiss Axiovert 200M inverted fluorescence microscope (20x/0.8 objective), with 512/25-nm excitation and 600/50 emission filters for DHE, and 475/28 nm excitation and 535/30 emission filters for HPF. Exposure time was 500 ms and 200 ms, for DHE and HPF, respectively. Images were acquired using a CCD camera (Cooled SNAP HQ, Photometrics), controlled by fluorescence imaging software (MetaFluor®, Molecular device). To quantify the intensity of the fluorescence signal, the images were analyzed using ImageJ software. After subtraction of the background noise, an average mean grey value was calculated from epidermal and cortical cells.

Endocytosis assay

For estimation of bulk endocytosis, seedlings were first pretreated in liquid MS/2 medium for 30 min in the absence or presence of the appropriate inhibitors. Seedlings were then transferred in 1 µM N-(3-triethylammoniumpropyl]-4[6-(4-(diethylamino)phenyl)hexatrienyl]pyridinium dibromide (FM4-64) in MS/2. After 7 min, the seedlings were washed in a liquid MS/2 medium deprived of FM4-64. They were then treated with 25 µM Brefeldin A (BFA) for 1 h, in the presence or absence of the appropriate inhibitors. To monitor the internalization of PIP2;1-GFP or GFP-AHA2, seedlings were treated for 45 min with 25 µM BFA. The number of BFA bodies per cell stained with FM4-64 or GFP was manually counted from images taken with a confocal microscope.

Confocal laser scanning microscopy

A Leica SP8 microscope with a 40x/1.1 water objective and the 488-nm line of its argon laser was used for live-cell imaging. Fluorescence emission was detected at 600-650 nm for FM4-64 and at 500-540 nm for GFP. To explore the full volume of epidermal cells, *z*-stacks of epidermal cell layers were made within 7 steps per acquisition, covering a 15-µm depth. For quantitative measurements of BFA bodies, the laser power, pinhole, and gain settings of the confocal microscope were identical among different treatments or genotypes.

sptPALM

Seedlings were transferred from vertically oriented plates to a petri dish containing MS/2 for 30 minutes, to allow recovery prior to incubation for 40 min in MS/2 complemented or not with 300 mM sorbitol. This last step was shortened to 15 min in the case of CLC2 experiments. Root cells were observed with a homemade TIRF microscope equipped with an emCCD camera (Andor iXON XU_897) and a 100x oil immersion objective (Apochromat NA = 1.45, Zeiss). Laser angle was selected to be close to supercritical angle and generate evanescent waves and to give the maximum signal-to-noise ratio (Konopka and Bednarek, 2008; Johnson and Vert, 2017). To ensure PALM localization of proteins, a continuous low-intensity illumination at 405 nm (OBIS LX 50mW Coherent) was used for photoactivation, while 561 nm (SAPPHIRE 100mW Coherent) with 600/50 (Chroma) emission filter was selected for image acquisition. The acquisition was steered by LabView software in streaming mode at 50 images/sec (20 msec exposure time). Ten thousand images were recorded per region of interest (ROI). From 10 to 20 ROIs were collected out of three biological replicates.

Single-particle tracking and Vonoroi tesselation

Individual single molecules were localized and tracked using a MTT software (Sergé et al., 2008). Dynamic properties of single emitters in root cells were then inferred from the tracks using homemade analysis software written in Matlab. From each track, the mean square displacement (MSD) was computed. In order to reduce the statistical noise while keeping a sufficiently high number of trajectories per cell, tracks of at least 5 steps (*i.e.* $\geq$ 6 localizations) were used. Missing frames due to mEOS blinking were allowed up to a maximum of three consecutive frames. The diffusion coefficient D was then calculated by fitting the MSD curve using the first four points. For the clustering analysis, the centroid of each individual track was calculated and used to implement SR-Tesseler software (Levet et al., 2015). Local densities of each track were calculated as the invert of their minimal surface.

Statistical analysis

For each condition or treatment, 9-12 cells were analyzed from at least 5-7 different seedlings. All experiments were independently repeated 2-3 times. Data are expressed as mean ± SE. Statistical analyses were performed in GraphPad Prism, using ANOVA followed by a Tukey's post hoc test or Student's *t*-test depending of the needs ($p<0.05$ was considered significant). Different letters in histograms indicate statistically different values.

Accession Numbers

Sequence data from this article can be found in the Arabidopsis Genome Initiative or GenBank/EMBL databases under the following accession numbers: *PIP2.1*, *At3G53420*; *AHA2*, *At4G30190*; *LTI6-b*, *At3G05890*; *CLC2*, *At2G40060*.

Supplemental Data

Supplemental Figure 1: Kinetics of DHE staining after a hyperosmotic treatment.

Supplemental Figure 2: ROS accumulation in root cells after a sorbitol treatment as revealed by hydroxyphenyl fluorescein (HPF)

Supplemental Figure 3: Diagram of experimental design.

Supplemental Figure 4: Effects of various sorbitol concentrations on cell plasmolysis and ROS accumulation.

Supplemental Figure 5: Localization using confocal microscopy of DHE fluorescence induced after 15 min of a mock or sorbitol treatment.

Supplemental Figure 6: Cell viability of root cells after a multiple inhibitor treatment (DPI plus BPDS).

Supplemental Figure 6: Lateral diffusion and local density of LTI6b-mEOS in response to a hyperosmotic sorbitol treatment.

Supplemental Figure 7: Effect of a hyperosmotic sorbitol treatment on PIP2;1-mEOS2 and mEOS-AHA2 cluster formation.

FIGURE LEGENDS

Figure 1: ROS accumulation in root cells after a sorbitol treatment. A, Schematic representation of ROS production as mediated by NADPH oxidases. B, ROS imaging using DHE fluorescence. Roots were incubated for 15 min with 5 µM DHE in the presence or absence of 300 mM sorbitol and subsequently observed under an epifluorescence microscope. The figure shows the red fluorescent signal induced upon oxidation of DHE. C, Quantification of DHE fluorescence in Col-0, *rbohD*, *rbohF*, and *rbohD/F* plants subjected or not to the sorbitol treatment. Effects on DHE fluorescence of a 30-min pretreatment, with either control (DMSO) or DPI, prior to incubation for 15 min with 5 µM DHE followed by a mock (no sorbitol) or 300 mM sorbitol treatment on Col-0 (D) or *rbohD/F* (F) plants. E, Schematic representation of ROS production by the putative ascorbate/iron pathway. G, Effects on DHE fluorescence of a 30-min pretreatment with BPDS (Fe^{2+} chelation) or AOX (ascorbate depletion), alone or in combination with DPI (RBOH inhibition). H, Effect of a 30-min pretreatment with BPDS on DHE fluorescence in the *rbohD/F* double mutant. I, Averaged DHE fluorescence intensity in Col-0 or *vtc2.4* roots incubated for 15 min in the presence or absence of sorbitol. DMSO represents a mock condition for comparison to a DPI pretreatment. J, Averaged DHE fluorescence intensity in control plants or plants treated with 100 µM ascorbate (Asc) for 15 min. Histograms show mean values ± SE (n = 38-211 cells). Different letters indicate statistically different values (ANOVA). Scale bars represent 20 µm.

Figure 2: Effects of hyperosmotic sorbitol treatment on bulk membrane and protein cargo internalization. A, Roots were pretreated with FM4-64 for 7 min followed by BFA for 1 h in the absence or presence of 300 mM sorbitol. FM4-64-labeled BFA bodies (arrows) indicate cellular bulk endocytosis. BFA bodies are more frequent in sorbitol-treated plants than in untreated plants, or plants cotreated with sorbitol, BPDS, and DPI. B, Average number of FM4-64-labeled BFA bodies per cells in control and sorbitol-treated plants. When indicated, plants were pretreated with BPDS and DPI, alone or in combination. C, Average number of FM4-64-labeled BFA bodies per cell in Col-0, *rbohD/F*, and *rbohD/F* plants treated with BPDS. D, Fluorescence intensity values shown in Figures 1C, 1D, and 1F were plotted against corresponding numbers of FM4-64-labeled BFA bodies per cell. A significant linear correlation ($R^2 = 0.71$) was observed. E and G, Confocal observation of root cells expressing Pro35S:GFP-AHA2 (E) or ProPIP2;1:PIP2;1-GFP (G) after a 45-min BFA treatment in the

presence (S) or absence (NS) of sorbitol. Only the ProPIP2;1:PIP2;1-GFP cells show a sorbitol-induced increase in GFP-labeled BFA bodies (arrows). F and H, Average number of GFP-AHA2- (F) or PIP2;1-GFP-labeled (H) BFA bodies per cell under control or sorbitol treatment conditions. For PIP2;1-GFP, the experiments were performed in the absence (Ctrl) or presence of a pretreatment with DPI or BPDS, alone or in combination. Histograms show means values ± SE (n =10-19). Scale bars represent 20 µm.

Figure 3: Effects of hyperosmotic sorbitol treatment on lateral diffusion of PIP2;1-mEOS and mEOS-AHA2. A and D, Track reconstructions in plants expressing ProPIP2;1:PIP2;1-mEOS (A) or ProUBQ10:mEOS-AHA2 (D), in the absence or presence of 300 mM sorbitol for 40 min. Each color represents a single molecule position over time. The right panels show close-up views of tracks in no sorbitol (NS) or sorbitol (S) conditions. B and E, Distribution of diffusion coefficients of PIP2;1-mEOS (B) and mEOS-AHA2 (E) in log scale. C and F, Mean diffusion coefficient values of PIP2;1-mEOS (C) and mEOS-AHA2 (F), in the absence or presence of sorbitol, and after treatment with the indicated inhibitors (DPI, BPDS, and DPI/BPDS). Histograms show mean values calculated from several thousands of individual tracks with SE (n = 12-30). Scale bars represent 1 µm.

Figure 4: Effects of hyperosmotic sorbitol treatment on local density of PIP2;1-mEOS and mEOS-AHA2. A and E, Super-resolution intensity map of PM of plants expressing ProPIP2;1:PIP2;1-mEOS (A) or ProUBQ10:mEOS-AHA2 (E), in the absence or presence of 300 mM sorbitol for 40 min. B and F, Local density distribution of PIP2;1-mEOS (B) or mEOS-AHA2 (F). C, Effects of DPI, BPDS, or their combination on the mean log value of local density of PIP2;1-mEOS, in the absence or presence of sorbitol. D, Effects of sorbitol on the mean log value of the local density of PIP2;1-mEOS in Col-0 or *rbohD* plants. Histograms show mean values calculated from several thousands of individual tracks with SE (n = 12-30). Scale bars represent 1 µm.

Figure 5: Effects of clathrin-mediated endocytosis on PIP2;1-GFP internalization and molecular dynamics of CLC2-mEOS in response to a hyperosmotic sorbitol treatment. A, Root cells coexpressing ProITAM>>HUB and Pro35S:PIP2;1-GFP in the presence of BFA for 45 min. PIP2;1-GFP labels BFA bodies in control conditions (left), but to a much lesser extent after induction of HUB with tamoxifen (Tam) (12 h), in the absence (center) or presence (right) of sorbitol. B, Super-resolution intensity map of PM of a plant expressing ProUBQ10:CLC2-mEOS, in the absence or presence of 300 mM sorbitol for 20 min. C, Local

density distribution of CLC2-mEOS. D, Track reconstruction in a ProUBQ10:CLC2-mEOS-expressing plant. Each color represents the displacement of a single molecule over time. Particles with a high (yellow) and low (blue) diffusion coefficient can be observed. E-F, Diffusion coefficient distribution of CLC2-mEOS, in the absence or presence of sorbitol, and in Col-0 (E) or *rbohD* (F). The gray box corresponds to the CLC2-mEOS mobile fraction. G, Corresponding graph showing the average percentage of CLC2-mEOS mobile fraction in Col-0 or *rbohD*, in the absence or presence of sorbitol. Histograms show mean values calculated from several thousands of individual tracks with SE (n > 15-31). Scale bars represent 1 µm.

Figure 6: Diagram of ROS signaling and its impact on protein dynamics after a hyperosmotic treatment. In control conditions, RBOHD/F (green) and putative efflux machinery (pink) for reducing power are inactive. A basal level of membrane internalization exists. CLC2 (brown) is either associated with AP2 (purple) in its diffusible form or is associated with CCVs, yielding nondiffusible forms. PIP2;1 (blue) and AHA2 (red) are organized in clusters and are mostly immobile. After a hyperosmotic treatment, activation of RBOHD/F and the efflux machinery (pink) for reducing power leads to enhanced production of superoxide. In the case of the reducing power efflux, this is achieved either by a direct efflux of cytoplasmic ascorbate (Asc) or an efflux or regeneration of dehydroascobate (DHA). The resulting reducing power reduces apoplastic transition metals, which in turn react with oxygen to generate ROS. The accumulation of ROS enhances lipid membrane internalization by an unknown mechanism. In parallel, ROS produced by RBOH facilitate plasma membrane association of CLC2/AP2 complexes by promoting interactions of AP2 with lipid at the membrane. An excess of these complexes can bind to PIP2;1, thereby facilitating its incorporation in CCVs. As a consequence, PIP2;1 clustering and endocytosis are enhanced. The rate of CLC2 dissociation from the CCV is intrinsically enhanced by the hyperosmotic stress, and this effect is compensated for by RBOH-dependent ROS and the above-mentioned effects on CL2/AP2 complex formation.

SUPPLEMENTAL FIGURE LEGENDS

Supplemental Figure 1: Kinetics of DHE staining after a hyperosmotic treatment. Roots were incubated with 5 µM DHE in the absence (empty symbols) or presence (filled symbols) of 300 mM sorbitol and observed for up to 120 min. The fluorescent signal shows a steady increase over time, which was always higher after a sorbitol treatment. Mean fluorescence intensity values ± SE (n >26).

Supplemental Figure 2: ROS accumulation in root cells after a sorbitol treatment as revealed by hydroxyphenyl fluorescein (HPF). A, Root cells stained with HPF for 15 min in the presence or absence of 300 mM sorbitol. B, Mean HPF fluorescence in response to sorbitol in roots pretreated for 30 min with DPI, BPDS, or their respective mock treatments (DMSO or ctrl). Histograms show mean fluorescence intensity values ± SE (n > 18). Scale bar represents 20 µm.

Supplemental Figure 3: Diagram of experimental design. Five-day-old seedlings were transferred in a liquid medium (MS/2, MES-KOH, pH 6, 1% sucrose) in the absence or presence of the indicated inhibitors. After 30 min, plants were incubated in the same liquid medium, but supplemented with DHE, and with or without sorbitol. Microscopy observation was performed after 15 min of this second treatment.

Supplemental Figure 4: Effects of various sorbitol concentrations on cell plasmolysis and ROS accumulation. A, Confocal observation of root cells expressing p35s:PIP2;1-GFP to reveal the PM and stained with propidium iodide (PI) to label the cell wall. In contrast to the 400 mM sorbitol treatment (see arrow heads), no plasmolysis was detected in control and 100 mM sorbitol conditions. In the presence of 300 mM sorbitol, an incipient plasmolysis can be observed (arrows). B, DHE fluorescence intensity (mean ± SEM) in plants incubated in the absence or presence of 100 mM sorbitol, without (Ctrl) or with DPI, BPDS, or AOX, alone or in combination (BPDS/DPI, AOX/DPI). WF, wide field. Scale bar represents 10 µm.

Supplemental Figure 5: Localization using confocal microscopy of DHE fluorescence induced after 15 min of a mock or sorbitol treatment. DHE stains the dotted structure (arrowheads) and nucleoli (star) in control cells and also in the apoplasm (arrows) after sorbitol treatment.

Supplemental Figure 6: Cell viability of root cells after a multiple inhibitor treatment (DPI plus BPDS). Plants were treated as explained for FM4-64 endocytosis test (Figure 3A, B, and

C) followed by an incubation with 3 µM FDA for 2 min. (A) FDA-induced fluorescent labeling of root cells. (B) Quantification of FDA fluorescence.

Supplemental Figure 6: Lateral diffusion and local density of LTI6b-mEOS in response to a hyperosmotic sorbitol treatment. A, Track reconstruction of ProUBQ10:LTI6b-mEOS. Each color represents the successive positions of one single molecule over time. The right panels show close-up views of tracks in the absence (NS) or presence (S) of sorbitol. B, Distribution of LTI6b-mEOS diffusion coefficient. C, Distribution of LTI6b-mEOS local density.

Supplemental Figure 7: Effect of a hyperosmotic sorbitol treatment on PIP2;1-mEOS2 and mEOS-AHA2 cluster formation. A, Average track density from simulated data or measurements in PIP2;1-mEOS2- or mEOS2-AHA2-expressing plants, in the absence or presence of 300 mM sorbitol. B, Vonoroi tessellation calculated from the position of each track centroid for simulated data or measurements in ProPIP2;1-PIP2;1-EOS- or ProUBQ10:mEOS2-AHA2-expressing cells, in the absence or presence of sorbitol. The smaller the polygons, the higher the local density of the detected molecule. C, Local density distribution of simulated data or particles detected in ProPIP2;1-PIP2;1-EOS- or ProUBQ10:mEOS2-AHA2-expressing plants.

ACKNOWLEDGMENTS

We thank the PHIV and MRI platform for access to microscopes, Jiri Friml for his kind HUB lines donation and Vincent Bayle for comment on the manuscript.

References

Baxter, A., Mittler, R., and Suzuki, N. (2014). ROS as key players in plant stress signalling. J. Exp. Bot. **65**: 1229–1240.

Ben Rejeb, K., Lefebvre-De Vos, D., Le Disquet, I., Leprince, A.-S., Bordenave, M., Maldiney, R., Jdey, A., Abdelly, C., and Savouré, A. (2015). Hydrogen peroxide produced by NADPH oxidases increases proline accumulation during salt or mannitol stress in Arabidopsis thaliana. New Phytol. **208**: 1138–1148.

Bruch, R.C. and Thayer, W.S. (1983). Differential effect of lipid peroxidation on membrane fluidity as determined by electron spin resonance probes. Biochim. Biophys. Acta **733**: 216–222.

Chen, J., Rogers, S.C., and Kavdia, M. (2013). Analysis of kinetics of dihydroethidium fluorescence with superoxide using xanthine oxidase and hypoxanthine assay. Ann. Biomed. Eng. **41**: 327–337.

Choi, W.-G., Toyota, M., Kim, S.-H., Hilleary, R., and Gilroy, S. (2014). Salt stress-induced Ca2+ waves are associated with rapid, long-distance root-to-shoot signaling in plants. Proc. Natl. Acad. Sci. U. S. A.

Clough, S.J. and Bent, A.F. (1998). Floral dip: a simplified method for Agrobacterium-mediated transformation of Arabidopsis thaliana. Plant J. Cell Mol. Biol. **16**: 735–743.

Davletova, S., Rizhsky, L., Liang, H., Shengqiang, Z., Oliver, D.J., Coutu, J., Shulaev, V., Schlauch, K., and Mittler, R. (2005). Cytosolic ascorbate peroxidase 1 is a central component of the reactive oxygen gene network of Arabidopsis. Plant Cell **17**: 268–281.

Dhonukshe, P., Aniento, F., Hwang, I., Robinson, D.G., Mravec, J., Stierhof, Y.-D., and Friml, J. (2007). Clathrin-mediated constitutive endocytosis of PIN auxin efflux carriers in Arabidopsis. Curr. Biol. CB **17**: 520–527.

Eichenberger, K., Böhni, P., Winterhalter, K.H., Kawato, S., and Richter, C. (1982). Microsomal lipid peroxidation causes an increase in the order of the membrane lipid domain. FEBS Lett. **142**: 59–62.

Feng, W., Lindner, H., Robbins, N.E., and Dinneny, J.R. (2016). Growing Out of Stress: The Role of Cell- and Organ-Scale Growth Control in Plant Water-Stress Responses. Plant Cell **28**: 1769–1782.

Gao, D., Knight, M.R., Trewavas, A.J., Sattelmacher, B., and Plieth, C. (2004). Self-reporting Arabidopsis expressing pH and [Ca2+] indicators unveil ion dynamics in the cytoplasm and in the apoplast under abiotic stress. Plant Physiol. **134**: 898–908.

Gaxiola, R.A., Palmgren, M.G., and Schumacher, K. (2007). Plant proton pumps. FEBS Lett. **581**: 2204–2214.

Geldner, N., Anders, N., Wolters, H., Keicher, J., Kornberger, W., Muller, P., Delbarre, A., Ueda, T., Nakano, A., and Jürgens, G. (2003). The Arabidopsis GNOM ARF-GEF mediates endosomal recycling, auxin transport, and auxin-dependent plant growth. Cell **112**: 219–230.

Gémes, K., Kim, Y.J., Park, K.Y., Moschou, P.N., Andronis, E., Valassaki, C., Roussis, A., and Roubelakis-Angelakis, K.A. (2016). An NADPH-Oxidase/Polyamine Oxidase Feedback Loop Controls Oxidative Burst Under Salinity. Plant Physiol. **172**: 1418–1431.

Grefen, C., Donald, N., Hashimoto, K., Kudla, J., Schumacher, K., and Blatt, M.R. (2010). A ubiquitin-10 promoter-based vector set for fluorescent protein tagging facilitates temporal stability and native protein distribution in transient and stable expression studies. Plant J. Cell Mol. Biol. **64**: 355–365.

Grillet, L., Ouerdane, L., Flis, P., Hoang, M.T.T., Isaure, M.-P., Lobinski, R., Curie, C., and Mari, S. (2014). Ascorbate efflux as a new strategy for iron reduction and transport in plants. J. Biol. Chem. **289**: 2515–2525.

Guo, K.-M., Babourina, O., and Rengel, Z. (2009). Na(+)/H(+) antiporter activity of the SOS1 gene: lifetime imaging analysis and electrophysiological studies on Arabidopsis seedlings. Physiol. Plant. **137**: 155–165.

Hamilton, E.S., Schlegel, A.M., and Haswell, E.S. (2015). United in diversity: mechanosensitive ion channels in plants. Annu. Rev. Plant Biol. **66**: 113–137.

Hao, H., Fan, L., Chen, T., Li, R., Li, X., He, Q., Botella, M.A., and Lin, J. (2014). Clathrin and Membrane Microdomains Cooperatively Regulate RbohD Dynamics and Activity in Arabidopsis. Plant Cell **26**: 1729–1745.

Haruta, M. and Sussman, M.R. (2012). The effect of a genetically reduced plasma membrane protonmotive force on vegetative growth of Arabidopsis. Plant Physiol. **158**: 1158–1171.

Haruta, M., Tan, L.X., Bushey, D.B., Swanson, S.J., and Sussman, M.R. (2018). Environmental and Genetic Factors Regulating Localization of the Plant Plasma Membrane H+-ATPase. Plant Physiol. **176**: 364–377.

Hosy, E., Martinière, A., Choquet, D., Maurel, C., and Luu, D.-T. (2015). Super-resolved and dynamic imaging of membrane proteins in plant cells reveal contrasting kinetic profiles and multiple confinement mechanisms. Mol. Plant **8**: 339–342.

Hou, C., Tian, W., Kleist, T., He, K., Garcia, V., Bai, F., Hao, Y., Luan, S., and Li, L. (2014). DUF221 proteins are a family of osmosensitive calcium-permeable cation channels conserved across eukaryotes. Cell Res. **24**: 632–635.

Jackson, L.P., Kelly, B.T., McCoy, A.J., Gaffry, T., James, L.C., Collins, B.M., Höning, S., Evans, P.R., and Owen, D.J. (2010). A large-scale conformational change couples membrane recruitment to cargo binding in the AP2 clathrin adaptor complex. Cell **141**: 1220–1229.

Jaillais, Y., Hothorn, M., Belkhadir, Y., Dabi, T., Nimchuk, Z.L., Meyerowitz, E.M., and Chory, J. (2011). Tyrosine phosphorylation controls brassinosteroid receptor activation by triggering membrane release of its kinase inhibitor. Genes Dev. **25**: 232–237.

Johnson, A. and Vert, G. (2017). Single Event Resolution of Plant Plasma Membrane Protein Endocytosis by TIRF Microscopy. Front. Plant Sci. **8**: 612.

Kadlecova, Z., Spielman, S.J., Loerke, D., Mohanakrishnan, A., Reed, D.K., and Schmid, S.L. (2016). Regulation of clathrin-mediated endocytosis by hierarchical allosteric activation of AP2. J Cell Biol: jcb.201608071.

Karimi, M., Bleys, A., Vanderhaeghen, R., and Hilson, P. (2007). Building Blocks for Plant Gene Assembly. Plant Physiol. **145**: 1183–1191.

Kelly, B.T., Graham, S.C., Liska, N., Dannhauser, P.N., Höning, S., Ungewickell, E.J., and Owen, D.J. (2014). Clathrin adaptors. AP2 controls clathrin polymerization with a membrane-activated switch. Science **345**: 459–463.

Konopka, C.A., Backues, S.K., and Bednarek, S.Y. (2008). Dynamics of Arabidopsis Dynamin-Related Protein 1C and a Clathrin Light Chain at the Plasma Membrane. Plant Cell **20**: 1363–1380.

Konopka, C.A. and Bednarek, S.Y. (2008). Variable-angle epifluorescence microscopy: a new way to look at protein dynamics in the plant cell cortex. Plant J. Cell Mol. Biol. **53**: 186–196.

Koussevitzky, S., Suzuki, N., Huntington, S., Armijo, L., Sha, W., Cortes, D., Shulaev, V., and Mittler, R. (2008). Ascorbate peroxidase 1 plays a key role in the response of Arabidopsis thaliana to stress combination. J. Biol. Chem. **283**: 34197–34203.

Lane, D.J.R., Robinson, S.R., Czerwinska, H., Bishop, G.M., and Lawen, A. (2010). Two routes of iron accumulation in astrocytes: ascorbate-dependent ferrous iron uptake via the divalent metal transporter (DMT1) plus an independent route for ferric iron. Biochem. J. **432**: 123–132.

Leborgne-Castel, N., Lherminier, J., Der, C., Fromentin, J., Houot, V., and Simon-Plas, F. (2008). The plant defense elicitor cryptogein stimulates clathrin-mediated endocytosis correlated with reactive oxygen species production in bright yellow-2 tobacco cells. Plant Physiol. **146**: 1255–1266.

Leshem, Y., Seri, L., and Levine, A. (2007). Induction of phosphatidylinositol 3-kinase-mediated endocytosis by salt stress leads to intracellular production of reactive oxygen species and salt tolerance. Plant J. Cell Mol. Biol. **51**: 185–197.

Levet, F., Hosy, E., Kechkar, A., Butler, C., Beghin, A., Choquet, D., and Sibarita, J.-B. (2015). SR-Tesseler: a method to segment and quantify localization-based super-resolution microscopy data. Nat. Methods **12**: 1065–1071.

Li, X., Wang, X., Yang, Y., Li, R., He, Q., Fang, X., Luu, D.-T., Maurel, C., and Lin, J. (2011). Single-molecule analysis of PIP2;1 dynamics and partitioning reveals multiple modes of Arabidopsis plasma membrane aquaporin regulation. Plant Cell **23**: 3780–3797.

Luu, D.-T., Martinière, A., Sorieul, M., Runions, J., and Maurel, C. (2012). Fluorescence recovery after photobleaching reveals high cycling dynamics of plasma membrane aquaporins in Arabidopsis roots under salt stress. Plant J. Cell Mol. Biol. **69**: 894–905.

Martinac, B., Buechner, M., Delcour, A.H., Adler, J., and Kung, C. (1987). Pressure-sensitive ion channel in Escherichia coli. Proc. Natl. Acad. Sci. U. S. A. **84**: 2297–2301.

Martinière, A. et al. (2012). Cell wall constrains lateral diffusion of plant plasma-membrane proteins. Proc. Natl. Acad. Sci. U. S. A. **109**: 12805–12810.

Mittler, R. (2017). ROS Are Good. Trends Plant Sci. **22**: 11–19.

Oparka, K.J. (1994). Plasmolysis: new insights into an old process. New Phytol. **126**: 571–591.

Pignocchi, C., Kiddle, G., Hernández, I., Foster, S.J., Asensi, A., Taybi, T., Barnes, J., and Foyer, C.H. (2006). Ascorbate oxidase-dependent changes in the redox state of the apoplast modulate gene transcript accumulation leading to modified hormone signaling and orchestration of defense processes in tobacco. Plant Physiol. **141**: 423–435.

Rodrigues, O., Reshetnyak, G., Grondin, A., Saijo, Y., Leonhardt, N., Maurel, C., and Verdoucq, L. (2017). Aquaporins facilitate hydrogen peroxide entry into guard cells to mediate ABA- and pathogen-triggered stomatal closure. Proc. Natl. Acad. Sci. U. S. A. **114**: 9200–9205.

Sandor, R., Der, C., Grosjean, K., Anca, I., Noirot, E., Leborgne-Castel, N., Lochman, J., Simon-Plas, F., and Gerbeau-Pissot, P. (2016). Plasma membrane order and fluidity are diversely triggered by elicitors of plant defence. J. Exp. Bot. **67**: 5173–5185.

Sergé, A., Bertaux, N., Rigneault, H., and Marguet, D. (2008). Dynamic multiple-target tracing to probe spatiotemporal cartography of cell membranes. Nat. Methods **5**: 687–694.

Stephan, A.B., Kunz, H.-H., Yang, E., and Schroeder, J.I. (2016). Rapid hyperosmotic-induced Ca2+ responses in Arabidopsis thaliana exhibit sensory potentiation and involvement of plastidial KEA transporters. Proc. Natl. Acad. Sci. U. S. A. **113**: E5242-5249.

Torres, M.A., Dangl, J.L., and Jones, J.D.G. (2002). Arabidopsis gp91phox homologues AtrbohD and AtrbohF are required for accumulation of reactive oxygen intermediates in the plant defense response. Proc. Natl. Acad. Sci. U. S. A. **99**: 517–522.

Tsukagoshi, H., Busch, W., and Benfey, P.N. (2010). Transcriptional regulation of ROS controls transition from proliferation to differentiation in the root. Cell **143**: 606–616.

Ueda, M., Tsutsumi, N., and Fujimoto, M. (2016). Salt stress induces internalization of plasma membrane aquaporin into the vacuole in Arabidopsis thaliana. Biochem. Biophys. Res. Commun. **474**: 742–746.

Urao, T., Yakubov, B., Satoh, R., Yamaguchi-Shinozaki, K., Seki, M., Hirayama, T., and Shinozaki, K. (1999). A Transmembrane Hybrid-Type Histidine Kinase in Arabidopsis Functions as an Osmosensor. Plant Cell **11**: 1743–1754.

Widholm, J.M. (1972). The use of fluorescein diacetate and phenosafranine for determining viability of cultured plant cells. Stain Technol. **47**: 189–194.

Wudick, M.M., Li, X., Valentini, V., Geldner, N., Chory, J., Lin, J., Maurel, C., and Luu, D.-T. (2015). Sub-cellular redistribution of root aquaporins induced by hydrogen peroxide. Mol. Plant.

Yuan, F. et al. (2014). OSCA1 mediates osmotic-stress-evoked Ca2+ increases vital for osmosensing in Arabidopsis. Nature **514**: 367–371.

Zwiewka, M., Nodzyński, T., Robert, S., Vanneste, S., and Friml, J. (2015). Osmotic Stress Modulates the Balance between Exocytosis and Clathrin-Mediated Endocytosis in Arabidopsis thaliana. Mol. Plant **8**: 1175–1187.

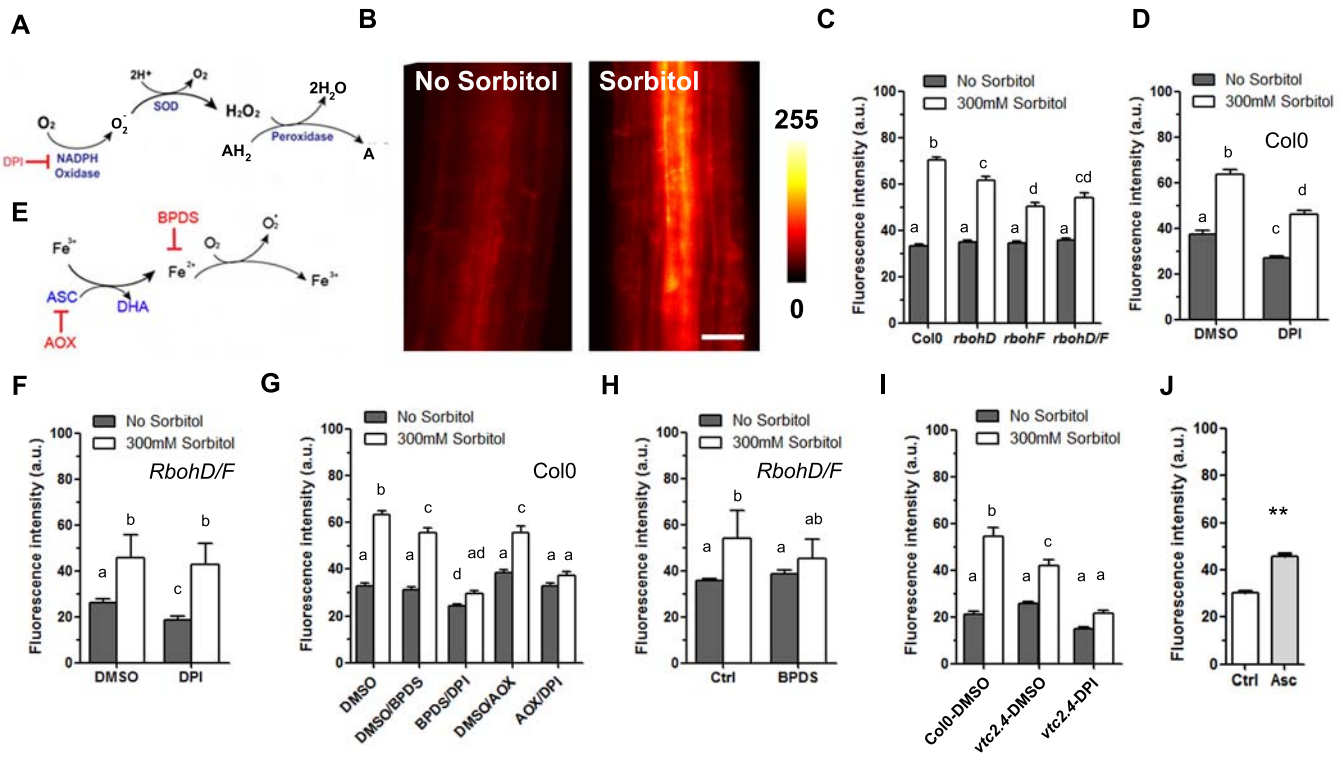

Figure 1: ROS accumulation in root cells after a sorbitol treatment. A, Schematic representation of ROS production as mediated by NADPH oxidases. B, ROS imaging using DHE fluorescence. Roots were incubated for 15 min with 5 µM DHE in the presence or absence of 300 mM sorbitol and subsequently observed under an epifluorescence microscope. The figure shows the red fluorescent signal induced upon oxidation of DHE. C, Quantification of DHE fluorescence in Col-0, rbohD, rbohF and rbohD/F plants subjected or not to the sorbitol treatment. Effects on DHE fluorescence of a 30 min pretreatment, either control (DMSO) or with DPI, prior to incubation for 15 min with 5µM DHE followed by a mock (no sorbitol) or 300 mM sorbitol treatment on Col0 (D) or rbohD/F (F) plant. E, Schematic representation of ROS production by the putative ascorbate/iron pathway. G, Effects on DHE fluorescence of a 30 min pretreatment with BPDS (Fe2+ chelation), or AOX (ascorbate depletion), alone or in combination with DPI (RBOH inhibition). H, Effect of a 30 min pretreatment with BPDS on DHE fluorescence in a rbohD/F double mutant. I, Averaged DHE fluorescence intensity in Col-0 or vtc2.4 roots incubated for 15 min in the presence or absence of sorbitol. DMSO represents a mock condition for comparison to a DPI pretreatment. J, Averaged DHE fluorescence intensity in control plants or plants treated with 100 µM ascorbate (Asc) for 15min. Histograms show mean values ±SEM (n = 38-211 cells). Different letters indicate statistically different values (ANOVA). Scale bars represent 20 µm.

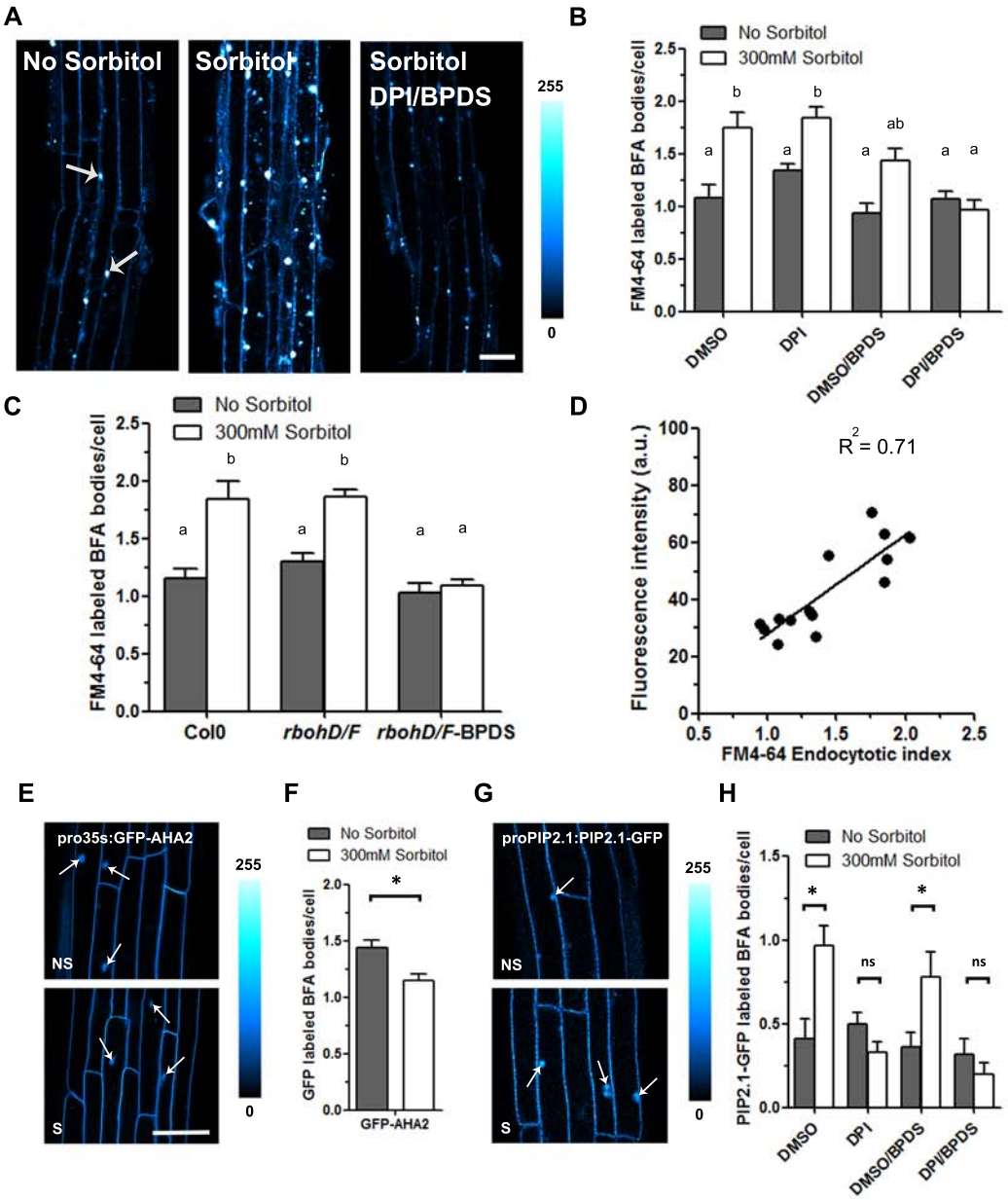

Figure 2: Effects of a hyperosmotic sorbitol treatment on bulk membrane and protein cargo internalization. A, Roots were pre-treated with FM4-64 for 7 min followed by BFA for 1 h in the absence or presence of 300 mM sorbitol. FM4-64 labeled BFA bodies (arrows) indicate cellular bulk endocytosis. BFA bodies are more frequent in sorbitol treated plants than in untreated plants, or plants co-treated with sorbitol, BPDS and DPI. B, Averaged number of FM4-64 labeled BFA bodies per cells in control and sorbitol treated plants. When indicated, plants were pretreated with BPDS and DPI, alone or in combination. C, Averaged number of FM4-64 labeled BFA bodies per cells in Col-0, rbohD/F and rbohD/F plants treated with BPDS. D, Fluorescence intensity values shown in Figures 1C, 1D and 1F were plotted against corresponding numbers of FM4-64 labeled BFA bodies per cells. A significant linear correlation (R2 = 0.71) can be observed. E and G, Confocal observation of root cells expressing Pro35S:GFP-AHA2 (E) or ProPIP2;1:PIP2;1-GFP (G) after a 45 min BFA treatment in the presence (S) or absence (NS) of sorbitol. Only the ProPIP2;1:PIP2;1-GFP cells show a sorbitol-induced increase in GFP-labeled BFA bodies (arrows). F and H, Averaged number of GFP-AHA2 (F) or PIP2;1-GFP (H) labeled BFA bodies per cell under control or sorbitol treatment conditions. For PIP2;1-GFP the experiments were performed in the absence (Ctrl) or presence of a pretreatment with DPI, BPDS, alone or a combination . Histograms show means values ± SEM (n =10-19). Scale bars represent 20 µm.

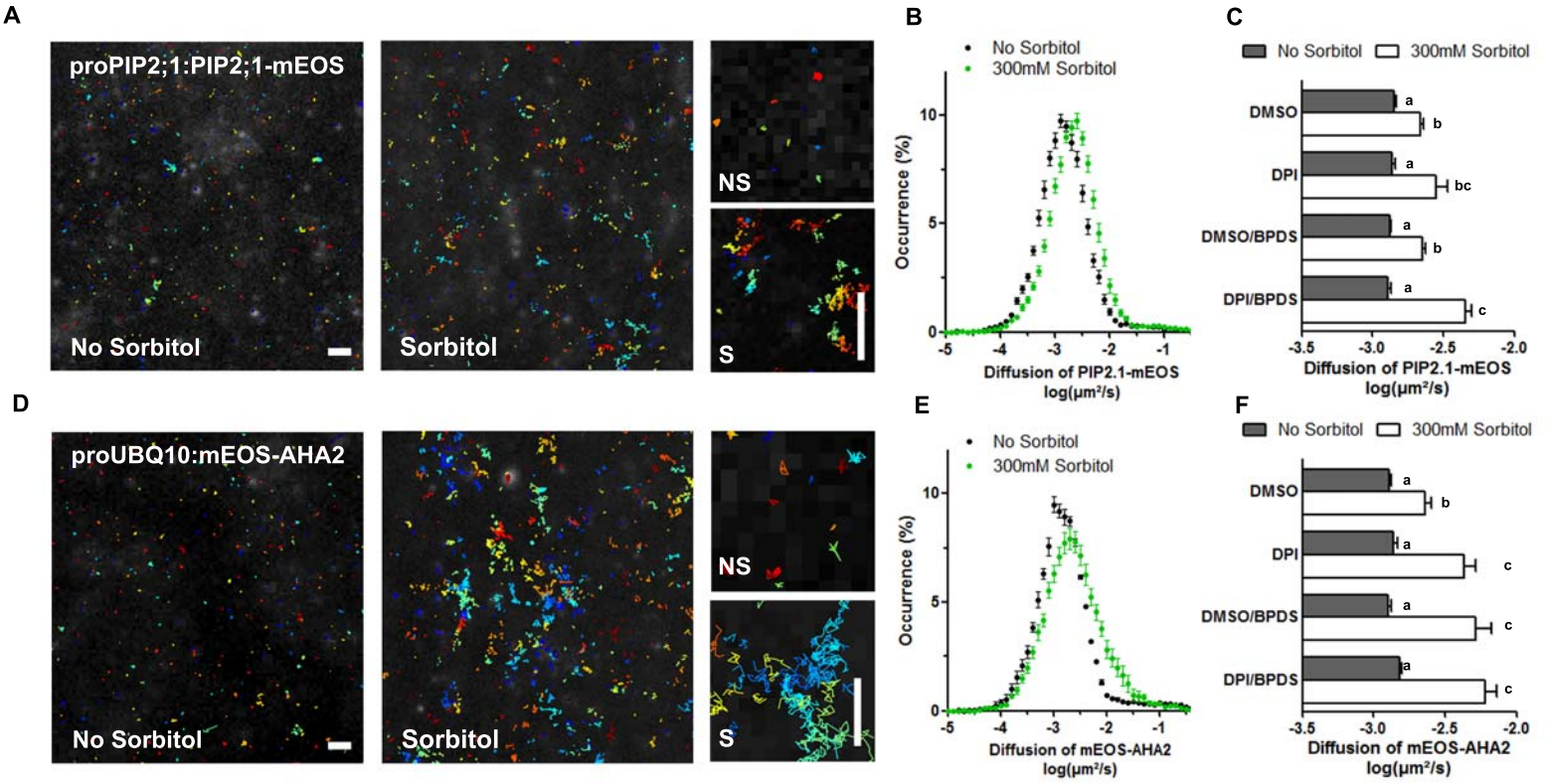

Figure 3: Effects of a hyperosmotic sorbitol treatment on lateral diffusion of PIP2;1-mEOS and mEOS-AHA2. A and D, Track reconstructions in plants expressing ProPIP2;1:PIP2;1-mEOS (A) or ProUBQ10:mEOS-AHA2 (D), in the absence or presence of 300mM sorbitol for 40min. Each color represents single molecule position over time. The right panels show close up views of tracks in no sorbitol (NS) or sorbitol (S) conditions. B and E, Distribution of diffusion coefficients of PIP2;1-mEOS (B) and mEOS-AHA2 (E) in log scale. C and F, Mean diffusion coefficient values of PIP2;1-mEOS (C) and mEOS-AHA2 (F), in the absence or presence of sorbitol, and after treatment with the indicated inhibitors (DPI, BPDS and DPI/BPDS). Histograms show mean values calculated from several thousands of individual tracks with SEM (n = 12-30). Scale bars represent 1 µm.

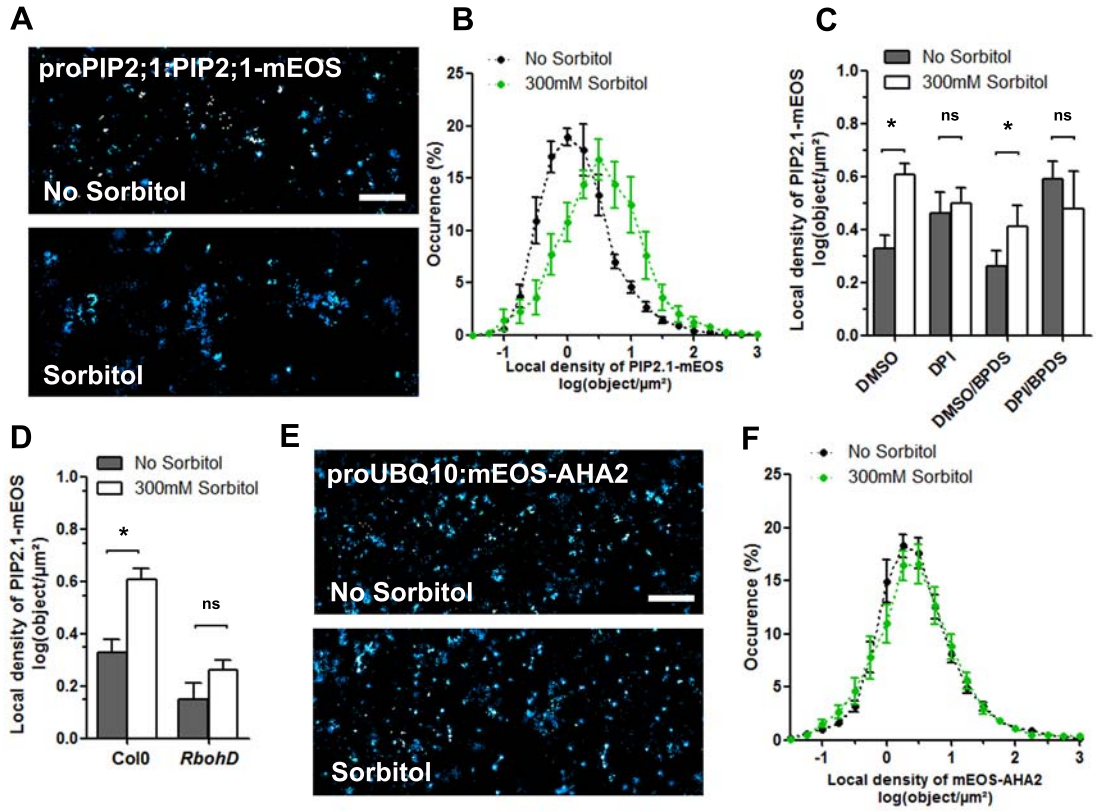

Figure 4: Effects of a hyperosmotic sorbitol treatment on local density of PIP2;1-mEOS and mEOS-AHA2. A and E, Super resolution intensity map of PM of plants expressing ProPIP2;1:PIP2;1-mEOS (A) or ProUBQ10:mEOS-AHA2 (E), in the absence or presence of 300mM sorbitol for 40 min. B and F, Local density distribution of PIP2;1-mEOS (B) or mEOS-AHA2 (F). C, Effects of DPI, BPDS or their combination on the mean log value of local density of PIP2;1-mEOS , in the absence or presence of sorbitol. D, Effects of sorbitol on the mean log value of the local density of PIP2;1-mEOS in Col-0 or rbohD plants. Histograms show mean values calculated from several thousands of individual tracks with SEM (n = 12-30). Scale bars represent 1 µm.

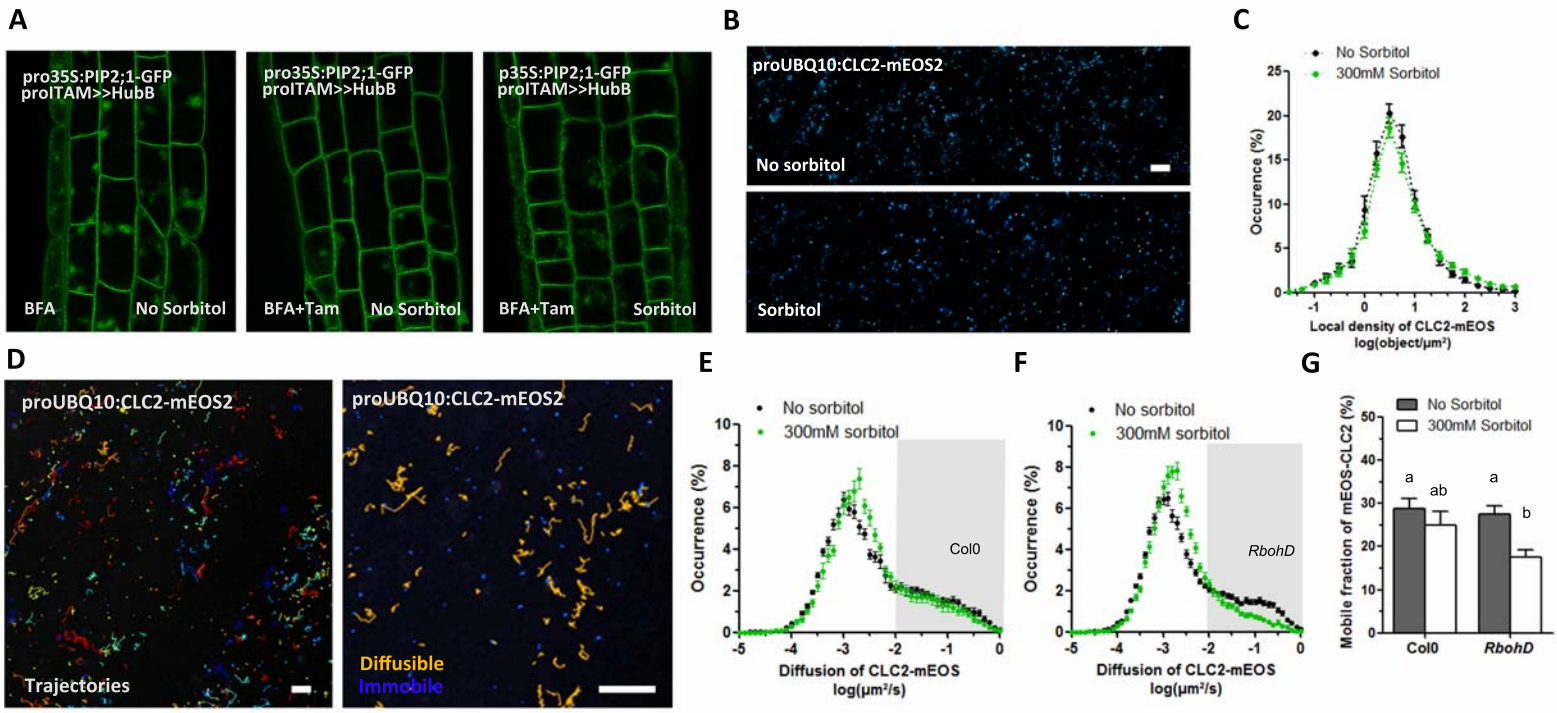

Figure 5: Effects of clathrin-mediated endocytosis on PIP2;1-GFP internalization and molecular dynamics of CLC2-mEOS in response to a hyper-osmotic sorbitol treatment. A, Root cells co-expressing ProITAM>>HUB and Pro35S:PIP2;1-GFP in the presence of BFA for 45 min. PIP2;1-GFP labels BFA bodies in control conditions (left), but to a much lesser extent after induction of HUB with tamoxifen (Tam) (12 h), in the absence (center) or presence (right) of sorbitol. B, Super resolution intensity map of PM of a plant expressing ProUBQ10:CLC2-mEOS, in the absence or presence of 300mM sorbitol for 20 min. C, Local density distribution of CLC2-mEOS. D, Track reconstruction in a ProUBQ10:CLC2-mEOS expressing plant. Each color represents the displacement of a single molecule over time. Particles with a high (yellow) and low (blue) diffusion coefficient can be observed. E-F, Diffusion coefficient distribution of CLC2-mEOS, in the absence or presence of sorbitol, and in Col-0 (E) or rbohD (F). The grey box corresponds to the CLC2-mEOS mobile fraction. G, Corresponding graph showing the average percentage of CLC2-mEOS mobile fraction in Col0 or rbohD, in the absence or presence of sorbitol. Histograms show mean values calculated from several thousands of individual tracks with SEM (n > 15-31). Scale bars represent 1 µm.

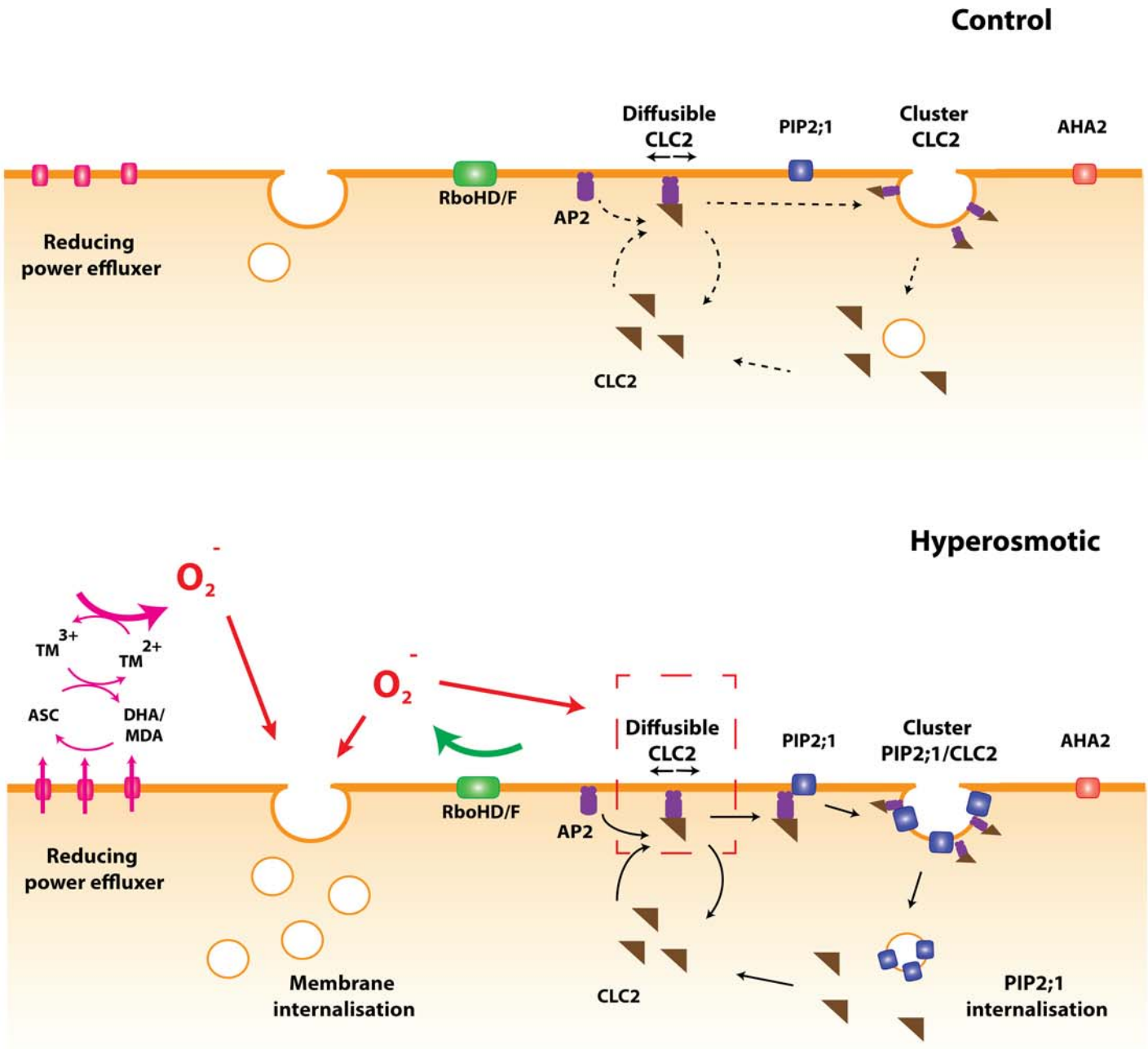

Figure 6: Diagram of ROS signaling and its impact on protein dynamics after a hyperosmotic treatment. In control conditions, RBOHD/F (green) and a putative efflux machinery (pink) for reducing power are inactive. A basal level of membrane internalization exists. CLC2 (brown) is either associated with AP2 (purple) in its diffusible form or is associated with CCVs, yielding non-diffusible forms. PIP2;1 (blue) and AHA2 (red) are organized in clusters and are mostly immobile. After a hyperosmotic treatment, activation of RBOHD/F and the efflux machinery (pink) for reducing power leads to enhanced production of super oxide. In the case of the reducing power efflux, this is achieved either by a direct efflux of cytoplasmic ascorbate (Asc), or an efflux or regeneration of dehydroascobate (DHA). The resulting reducing power reduces apoplastic transition metals, which in turn react with oxygen to generate ROS. The accumulation of ROS enhances lipid membrane internalization by an unknown mechanism. In parallel, ROS produced by RBOH facilitate plasma membrane association of CLC2/AP2 complexes by promoting interactions of AP2 with lipid at the membrane. An excess of these complexes can bind to PIP2;1, thereby facilitating its incorporation in CCVs. As a consequence, PIP2;1 clustering and endocytosis is enhanced. The rate of CLC2 dissociation from the CCV is intrinsically enhanced by the hyperosmotic stress, this effect being compensated by RBOH-dependent ROS and the above mentioned effects on CL2/AP2 complex formation.

Parsed Citations

Baxter, A., Mittler, R., and Suzuki, N. (2014). ROS as key players in plant stress signalling. J. Exp. Bot. 65: 1229–1240.
Pubmed: Author and Title
Google Scholar: Author Only Title Only Author and Title

Ben Rejeb, K., Lefebvre-De Vos, D., Le Disquet, I., Leprince, A.-S., Bordenave, M., Maldiney, R., Jdey, A., Abdelly, C., and Savouré, A. (2015). Hydrogen peroxide produced by NADPH oxidases increases proline accumulation during salt or mannitol stress in Arabidopsis thaliana. New Phytol. 208: 1138–1148.
Pubmed: Author and Title
Google Scholar: Author Only Title Only Author and Title

Bruch, R.C. and Thayer, W.S. (1983). Differential effect of lipid peroxidation on membrane fluidity as determined by electron spin resonance probes. Biochim. Biophys. Acta 733: 216–222.
Pubmed: Author and Title
Google Scholar: Author Only Title Only Author and Title

Chen, J., Rogers, S.C., and Kavdia, M. (2013). Analysis of kinetics of dihydroethidium fluorescence with superoxide using xanthine oxidase and hypoxanthine assay. Ann. Biomed. Eng. 41: 327–337.
Pubmed: Author and Title
Google Scholar: Author Only Title Only Author and Title

Choi, W.-G., Toyota, M., Kim, S.-H., Hilleary, R., and Gilroy, S. (2014). Salt stress-induced Ca2+ waves are associated with rapid, long-distance root-to-shoot signaling in plants. Proc. Natl. Acad. Sci. U. S. A.
Pubmed: Author and Title
Google Scholar: Author Only Title Only Author and Title

Clough, S.J. and Bent, A.F. (1998). Floral dip: a simplified method for Agrobacterium-mediated transformation of Arabidopsis thaliana. Plant J. Cell Mol. Biol. 16: 735–743.
Pubmed: Author and Title
Google Scholar: Author Only Title Only Author and Title

Davletova, S., Rizhsky, L., Liang, H., Shengqiang, Z., Oliver, D.J., Coutu, J., Shulaev, V., Schlauch, K., and Mittler, R. (2005). Cytosolic ascorbate peroxidase 1 is a central component of the reactive oxygen gene network of Arabidopsis. Plant Cell 17: 268–281.
Pubmed: Author and Title
Google Scholar: Author Only Title Only Author and Title

Dhonukshe, P., Aniento, F., Hwang, I., Robinson, D.G., Mravec, J., Stierhof, Y.-D., and Friml, J. (2007). Clathrin-mediated constitutive endocytosis of PIN auxin efflux carriers in Arabidopsis. Curr. Biol. CB 17: 520–527.
Pubmed: Author and Title
Google Scholar: Author Only Title Only Author and Title

Eichenberger, K., Böhni, P., Winterhalter, K.H., Kawato, S., and Richter, C. (1982). Microsomal lipid peroxidation causes an increase in the order of the membrane lipid domain. FEBS Lett. 142: 59–62.
Pubmed: Author and Title
Google Scholar: Author Only Title Only Author and Title

Feng, W., Lindner, H., Robbins, N.E., and Dinneny, J.R. (2016). Growing Out of Stress: The Role of Cell- and Organ-Scale Growth Control in Plant Water-Stress Responses. Plant Cell 28: 1769–1782.
Pubmed: Author and Title
Google Scholar: Author Only Title Only Author and Title

Gao, D., Knight, M.R., Trewavas, A.J., Sattelmacher, B., and Plieth, C. (2004). Self-reporting Arabidopsis expressing pH and [Ca2+] indicators unveil ion dynamics in the cytoplasm and in the apoplast under abiotic stress. Plant Physiol. 134: 898–908.
Pubmed: Author and Title
Google Scholar: Author Only Title Only Author and Title

Gaxiola, R.A., Palmgren, M.G., and Schumacher, K. (2007). Plant proton pumps. FEBS Lett. 581: 2204–2214.
Pubmed: Author and Title
Google Scholar: Author Only Title Only Author and Title

Geldner, N., Anders, N., Wolters, H., Keicher, J., Kornberger, W., Muller, P., Delbarre, A., Ueda, T., Nakano, A., and Jürgens, G. (2003). The Arabidopsis GNOM ARF-GEF mediates endosomal recycling, auxin transport, and auxin-dependent plant growth. Cell 112: 219–230.
Pubmed: Author and Title
Google Scholar: Author Only Title Only Author and Title

Gémes, K., Kim, Y.J., Park, K.Y., Moschou, P.N., Andronis, E., Valassaki, C., Roussis, A., and Roubelakis-Angelakis, K.A. (2016). An NADPH-Oxidase/Polyamine Oxidase Feedback Loop Controls Oxidative Burst Under Salinity. Plant Physiol. 172: 1418–1431.
Pubmed: Author and Title
Google Scholar: Author Only Title Only Author and Title

Grefen, C., Donald, N., Hashimoto, K., Kudla, J., Schumacher, K., and Blatt, M.R. (2010). A ubiquitin-10 promoter-based vector set for fluorescent protein tagging facilitates temporal stability and native protein distribution in transient and stable expression studies.

Plant J. Cell Mol. Biol. 64: 355–365.
Pubmed: Author and Title
Google Scholar: Author Only Title Only Author and Title

Grillet, L., Ouerdane, L., Flis, P., Hoang, M.T.T., Isaure, M.-P., Lobinski, R., Curie, C., and Mari, S. (2014). Ascorbate efflux as a new strategy for iron reduction and transport in plants. J. Biol. Chem. 289: 2515–2525.
Pubmed: Author and Title
Google Scholar: Author Only Title Only Author and Title

Guo, K.-M., Babourina, O., and Rengel, Z. (2009). Na(+)/H(+) antiporter activity of the SOS1 gene: lifetime imaging analysis and electrophysiological studies on Arabidopsis seedlings. Physiol. Plant. 137: 155–165.
Pubmed: Author and Title
Google Scholar: Author Only Title Only Author and Title

Hamilton, E.S., Schlegel, A.M., and Haswell, E.S. (2015). United in diversity: mechanosensitive ion channels in plants. Annu. Rev. Plant Biol. 66: 113–137.
Pubmed: Author and Title
Google Scholar: Author Only Title Only Author and Title

Hao, H., Fan, L., Chen, T., Li, R., Li, X., He, Q., Botella, M.A., and Lin, J. (2014). Clathrin and Membrane Microdomains Cooperatively Regulate RbohD Dynamics and Activity in Arabidopsis. Plant Cell 26: 1729–1745.
Pubmed: Author and Title
Google Scholar: Author Only Title Only Author and Title

Haruta, M. and Sussman, M.R. (2012). The effect of a genetically reduced plasma membrane protonmotive force on vegetative growth of Arabidopsis. Plant Physiol. 158: 1158–1171.
Pubmed: Author and Title
Google Scholar: Author Only Title Only Author and Title

Haruta, M., Tan, L.X., Bushey, D.B., Swanson, S.J., and Sussman, M.R. (2018). Environmental and Genetic Factors Regulating Localization of the Plant Plasma Membrane H+-ATPase. Plant Physiol. 176: 364–377.
Pubmed: Author and Title
Google Scholar: Author Only Title Only Author and Title

Hosy, E., Martinière, A., Choquet, D., Maurel, C., and Luu, D.-T. (2015). Super-resolved and dynamic imaging of membrane proteins in plant cells reveal contrasting kinetic profiles and multiple confinement mechanisms. Mol. Plant 8: 339–342.
Pubmed: Author and Title
Google Scholar: Author Only Title Only Author and Title

Hou, C., Tian, W., Kleist, T., He, K., Garcia, V., Bai, F., Hao, Y., Luan, S., and Li, L. (2014). DUF221 proteins are a family of osmosensitive calcium-permeable cation channels conserved across eukaryotes. Cell Res. 24: 632–635.
Pubmed: Author and Title
Google Scholar: Author Only Title Only Author and Title

Jackson, L.P., Kelly, B.T., McCoy, A.J., Gaffry, T., James, L.C., Collins, B.M., Höning, S., Evans, P.R., and Owen, D.J. (2010). A large-scale conformational change couples membrane recruitment to cargo binding in the AP2 clathrin adaptor complex. Cell 141: 1220–1229.
Pubmed: Author and Title
Google Scholar: Author Only Title Only Author and Title

Jaillais, Y., Hothorn, M., Belkhadir, Y., Dabi, T., Nimchuk, Z.L., Meyerowitz, E.M., and Chory, J. (2011). Tyrosine phosphorylation controls brassinosteroid receptor activation by triggering membrane release of its kinase inhibitor. Genes Dev. 25: 232–237.
Pubmed: Author and Title
Google Scholar: Author Only Title Only Author and Title

Johnson, A. and Vert, G. (2017). Single Event Resolution of Plant Plasma Membrane Protein Endocytosis by TIRF Microscopy. Front. Plant Sci. 8: 612.
Pubmed: Author and Title
Google Scholar: Author Only Title Only Author and Title

Kadlecova, Z., Spielman, S.J., Loerke, D., Mohanakrishnan, A., Reed, D.K., and Schmid, S.L. (2016). Regulation of clathrin-mediated endocytosis by hierarchical allosteric activation of AP2. J Cell Biol: jcb.201608071.
Pubmed: Author and Title
Google Scholar: Author Only Title Only Author and Title

Karimi, M., Bleys, A., Vanderhaeghen, R., and Hilson, P. (2007). Building Blocks for Plant Gene Assembly. Plant Physiol. 145: 1183–1191.
Pubmed: Author and Title
Google Scholar: Author Only Title Only Author and Title

Kelly, B.T., Graham, S.C., Liska, N., Dannhauser, P.N., Höning, S., Ungewickell, E.J., and Owen, D.J. (2014). Clathrin adaptors. AP2 controls clathrin polymerization with a membrane-activated switch. Science 345: 459–463.
Pubmed: Author and Title
Google Scholar: Author Only Title Only Author and Title

Konopka, C.A., Backues, S.K., and Bednarek, S.Y. (2008). Dynamics of Arabidopsis Dynamin-Related Protein 1C and a Clathrin Light Chain at the Plasma Membrane. Plant Cell 20: 1363–1380.

Pubmed: Author and Title
Google Scholar: Author Only Title Only Author and Title

Konopka, C.A. and Bednarek, S.Y. (2008). Variable-angle epifluorescence microscopy: a new way to look at protein dynamics in the plant cell cortex. Plant J. Cell Mol. Biol. 53: 186–196.
Pubmed: Author and Title
Google Scholar: Author Only Title Only Author and Title

Koussevitzky, S., Suzuki, N., Huntington, S., Armijo, L., Sha, W., Cortes, D., Shulaev, V., and Mittler, R. (2008). Ascorbate peroxidase 1 plays a key role in the response of Arabidopsis thaliana to stress combination. J. Biol. Chem. 283: 34197–34203.
Pubmed: Author and Title
Google Scholar: Author Only Title Only Author and Title

Lane, D.J.R., Robinson, S.R., Czerwinska, H., Bishop, G.M., and Lawen, A. (2010). Two routes of iron accumulation in astrocytes: ascorbate-dependent ferrous iron uptake via the divalent metal transporter (DMT1) plus an independent route for ferric iron. Biochem. J. 432: 123–132.
Pubmed: Author and Title
Google Scholar: Author Only Title Only Author and Title

Leborgne-Castel, N., Lherminier, J., Der, C., Fromentin, J., Houot, V., and Simon-Plas, F. (2008). The plant defense elicitor cryptogein stimulates clathrin-mediated endocytosis correlated with reactive oxygen species production in bright yellow-2 tobacco cells. Plant Physiol. 146: 1255–1266.
Pubmed: Author and Title
Google Scholar: Author Only Title Only Author and Title

Leshem, Y., Seri, L., and Levine, A. (2007). Induction of phosphatidylinositol 3-kinase-mediated endocytosis by salt stress leads to intracellular production of reactive oxygen species and salt tolerance. Plant J. Cell Mol. Biol. 51: 185–197.
Pubmed: Author and Title
Google Scholar: Author Only Title Only Author and Title

Levet, F., Hosy, E., Kechkar, A., Butler, C., Beghin, A., Choquet, D., and Sibarita, J.-B. (2015). SR-Tesseler: a method to segment and quantify localization-based super-resolution microscopy data. Nat. Methods 12: 1065–1071.
Pubmed: Author and Title
Google Scholar: Author Only Title Only Author and Title

Li, X., Wang, X., Yang, Y., Li, R., He, Q., Fang, X., Luu, D.-T., Maurel, C., and Lin, J. (2011). Single-molecule analysis of PIP2;1 dynamics and partitioning reveals multiple modes of Arabidopsis plasma membrane aquaporin regulation. Plant Cell 23: 3780–3797.
Pubmed: Author and Title
Google Scholar: Author Only Title Only Author and Title

Luu, D.-T., Martinière, A., Sorieul, M., Runions, J., and Maurel, C. (2012). Fluorescence recovery after photobleaching reveals high cycling dynamics of plasma membrane aquaporins in Arabidopsis roots under salt stress. Plant J. Cell Mol. Biol. 69: 894–905.
Pubmed: Author and Title
Google Scholar: Author Only Title Only Author and Title

Martinac, B., Buechner, M., Delcour, A.H., Adler, J., and Kung, C. (1987). Pressure-sensitive ion channel in Escherichia coli. Proc. Natl. Acad. Sci. U. S. A. 84: 2297–2301.
Pubmed: Author and Title
Google Scholar: Author Only Title Only Author and Title

Martinière, A. et al. (2012). Cell wall constrains lateral diffusion of plant plasma-membrane proteins. Proc. Natl. Acad. Sci. U. S. A. 109: 12805–12810.
Pubmed: Author and Title
Google Scholar: Author Only Title Only Author and Title

Mittler, R. (2017). ROS Are Good. Trends Plant Sci. 22: 11–19.
Pubmed: Author and Title
Google Scholar: Author Only Title Only Author and Title

Oparka, K.J. (1994). Plasmolysis: new insights into an old process. New Phytol. 126: 571–591.
Pubmed: Author and Title
Google Scholar: Author Only Title Only Author and Title

Pignocchi, C., Kiddle, G., Hernández, I., Foster, S.J., Asensi, A., Taybi, T., Barnes, J., and Foyer, C.H. (2006). Ascorbate oxidase-dependent changes in the redox state of the apoplast modulate gene transcript accumulation leading to modified hormone signaling and orchestration of defense processes in tobacco. Plant Physiol. 141: 423–435.
Pubmed: Author and Title
Google Scholar: Author Only Title Only Author and Title

Rodrigues, O., Reshetnyak, G., Grondin, A., Saijo, Y., Leonhardt, N., Maurel, C., and Verdoucq, L. (2017). Aquaporins facilitate hydrogen peroxide entry into guard cells to mediate ABA- and pathogen-triggered stomatal closure. Proc. Natl. Acad. Sci. U. S. A. 114: 9200–9205.
Pubmed: Author and Title
Google Scholar: Author Only Title Only Author and Title

Sandor, R., Der, C., Grosjean, K., Anca, I., Noirot, E., Leborgne-Castel, N., Lochman, J., Simon-Plas, F., and Gerbeau-Pissot, P. (2016).

Plasma membrane order and fluidity are diversely triggered by elicitors of plant defence. J. Exp. Bot. 67: 5173–5185.
Pubmed: Author and Title
Google Scholar: Author Only Title Only Author and Title

Sergé, A., Bertaux, N., Rigneault, H., and Marguet, D. (2008). Dynamic multiple-target tracing to probe spatiotemporal cartography of cell membranes. Nat. Methods 5: 687–694.
Pubmed: Author and Title
Google Scholar: Author Only Title Only Author and Title

Stephan, A.B., Kunz, H.-H., Yang, E., and Schroeder, J.I. (2016). Rapid hyperosmotic-induced Ca2+ responses in Arabidopsis thaliana exhibit sensory potentiation and involvement of plastidial KEA transporters. Proc. Natl. Acad. Sci. U. S. A. 113: E5242-5249.
Pubmed: Author and Title
Google Scholar: Author Only Title Only Author and Title

Torres, M.A., Dangl, J.L., and Jones, J.D.G. (2002). Arabidopsis gp91phox homologues AtrbohD and AtrbohF are required for accumulation of reactive oxygen intermediates in the plant defense response. Proc. Natl. Acad. Sci. U. S. A. 99: 517–522.
Pubmed: Author and Title
Google Scholar: Author Only Title Only Author and Title

Tsukagoshi, H., Busch, W., and Benfey, P.N. (2010). Transcriptional regulation of ROS controls transition from proliferation to differentiation in the root. Cell 143: 606–616.
Pubmed: Author and Title
Google Scholar: Author Only Title Only Author and Title

Ueda, M., Tsutsumi, N., and Fujimoto, M. (2016). Salt stress induces internalization of plasma membrane aquaporin into the vacuole in Arabidopsis thaliana. Biochem. Biophys. Res. Commun. 474: 742–746.
Pubmed: Author and Title
Google Scholar: Author Only Title Only Author and Title

Urao, T., Yakubov, B., Satoh, R., Yamaguchi-Shinozaki, K., Seki, M., Hirayama, T., and Shinozaki, K. (1999). A Transmembrane Hybrid-Type Histidine Kinase in Arabidopsis Functions as an Osmosensor. Plant Cell 11: 1743–1754.
Pubmed: Author and Title
Google Scholar: Author Only Title Only Author and Title

Widholm, J.M. (1972). The use of fluorescein diacetate and phenosafranine for determining viability of cultured plant cells. Stain Technol. 47: 189–194.
Pubmed: Author and Title
Google Scholar: Author Only Title Only Author and Title

Wudick, M.M., Li, X., Valentini, V., Geldner, N., Chory, J., Lin, J., Maurel, C., and Luu, D.-T. (2015). Sub-cellular redistribution of root aquaporins induced by hydrogen peroxide. Mol. Plant.
Pubmed: Author and Title
Google Scholar: Author Only Title Only Author and Title

Yuan, F. et al. (2014). OSCA1 mediates osmotic-stress-evoked Ca2+ increases vital for osmosensing in Arabidopsis. Nature 514: 367–371.
Pubmed: Author and Title
Google Scholar: Author Only Title Only Author and Title

Zwiewka, M., Nodzyński, T., Robert, S., Vanneste, S., and Friml, J. (2015). Osmotic Stress Modulates the Balance between Exocytosis and Clathrin-Mediated Endocytosis in Arabidopsis thaliana. Mol. Plant 8: 1175–1187.
Pubmed: Author and Title
Google Scholar: Author Only Title Only Author and Title